



Corrosion of porous Mg and Fe scaffolds: a review of mechanical and biocompatibility responses

Abdul Hakim Md Yusop, Ahmed Alsakkaf, Mohammed Rafiq Abdul Kadir, Irza Sukmana & Hadi Nur

To cite this article: Abdul Hakim Md Yusop, Ahmed Alsakkaf, Mohammed Rafiq Abdul Kadir, Irza Sukmana & Hadi Nur (2021) Corrosion of porous Mg and Fe scaffolds: a review of mechanical and biocompatibility responses, Corrosion Engineering, Science and Technology, 56:4, 310-326, DOI: [10.1080/1478422X.2021.1879427](https://doi.org/10.1080/1478422X.2021.1879427)

To link to this article: <https://doi.org/10.1080/1478422X.2021.1879427>



Published online: 10 Feb 2021.



Submit your article to this journal [↗](#)



Article views: 128



View related articles [↗](#)



View Crossmark data [↗](#)

Corrosion of porous Mg and Fe scaffolds: a review of mechanical and biocompatibility responses

Abdul Hakim Md Yusop^a, Ahmed Alsakkaf^b, Mohammed Rafiq Abdul Kadir^c, Irza Sukmana^d and Hadi Nur^{a,e}

^aCenter for Sustainable Nanomaterials, Ibnu Sina Institute for Scientific and Industrial Research, Universiti Teknologi Malaysia, Johor, Malaysia; ^bSchool of Mechanical Engineering, Universiti Teknologi Malaysia, Johor, Malaysia; ^cMedical Implant Technology Center, Faculty of Engineering, Universiti Teknologi Malaysia, Johor, Malaysia; ^dDepartment of Mechanical Engineering, Lampung University, Lampung, Indonesia; ^eCentral Laboratory of Minerals and Advanced Materials, Faculty of Mathematics and Natural Sciences, State University of Malang, Malang, Indonesia

ABSTRACT

Absorbable metals have been proposed as potential materials for hard tissue scaffolding to offer both high mechanical support and bioabsorbability. Over the past 5 years, many works sought evidence of the interesting mechanical property which mimics that of human bone with tailored corrosion behaviour. The emerging additive manufacturing (AM) technology helps to optimise the design and production of topological porous absorbable metals suited for bone scaffolds. Since the studies on the porous absorbable metals are on the rise, we provide a current state-of-the-art of corrosion performances for porous Mg-based and Fe-based scaffolds including recent developments and the remaining challenges. A detailed discussion on the impacts of advanced AM and recently developed dynamic-flow corrosion on their *in vitro* corrosion, mechanical strengths and biocompatibility are also provided. This review also analyses the suitability of both metals to be used for bone substitute materials.

ARTICLE HISTORY

Received 11 November 2020
Accepted 18 January 2021

KEYWORDS

Corrosion; porous Mg; porous Fe; bone; scaffolds; mechanical integrity; biocompatibility

Introduction

An ideal tissue-engineered scaffold is a three-dimensional bioactive and absorbable porous solid structure that plays a crucial role in assisting tissue regeneration [1]. At a certain point, when the strength of polymers is insufficient and the brittleness of ceramics becomes problematic, absorbable metals offer both strength and ductility [2]. High mechanical strength endowed by metals renders them a suitable scaffolding material for load transfer without resulting in large deformations and permanent dimensional changes [3]. To date, iron (Fe), magnesium (Mg), zinc (Zn) and their alloys are the current types of absorbable metals. The advent of these metals in biomedical applications has shifted the established paradigm of metal implants from preventing corrosion to its direct application. An absorbable metal implant allows the replacement of biological tissues via physiological extracellular components without leaving toxic corrosion products [4]. Its corrosion rate can be matched to the rate of new tissue regeneration to maintain the structural integrity and to provide a smooth transition of the load transfer from the scaffold to the tissue.

Figure 1 presents the characteristics of the ideal bone scaffold. In order for the bone scaffold to assist in tissue regeneration effectively, it should be able to promote cell–biomaterial interactions, cell proliferation, adhesion, growth, migration and differentiation, and permits transportation for nutrients, gases and waste removal for cell survival. Besides having a high porosity and pore interconnectivity, the scaffolds should possess adequate mechanical strength and corrode at a rate that is congruent with tissue healing time. Convenient to be designed and surface-treated are also included in the ideal properties of a scaffold.

Over the past 8 years, more works on these new types of biomaterials have been published. This is demonstrated by the rapid increase in scientific publication, progressive development of standards and launching of the first commercial products. The emerging additive manufacturing (AM) technology helps to advance the design and process of topological porous metals suited for bone scaffolds and orthopaedic implants [5]. In the light of the increasing interest on the porous absorbable metals, we provide a current state-of-the-art of porous Mg-based and Fe-based scaffolds including recent developments and the remaining challenges. We also present the recent status of both metals in advanced AM and dynamic-flow corrosion and provide a detailed look at how far did these new parameters affect the corrosion, mechanical properties and the biocompatibility of both metals in their porous structure. This review provides an insight into the current status of porous Mg-based and Fe-based scaffolds as well as presenting some strategies to cope with the remaining challenges.

Mg corrosion behaviour

Although early applications considered magnesium biocorrosion properties as a disadvantage, this metal has a long history of promising use as an implant material owing to its weight and mechanical strength [6,7]. Mg and its alloys are very lightweight metals having density ranging from 1.74 to 2.0 g cm⁻³, which is less than that of titanium (Ti) alloys (4.4–4.5 g cm⁻³) and stainless steel (SS) 316 L (8.0 g cm⁻³). Interestingly, the weight of Mg and its alloys is close to that of cortical bone (1.8–2.1 g cm⁻³) and cancellous bone (1.0–1.4 g cm⁻³) [8]. Moreover, Mg possesses appropriate mechanical strength that is close to the cortical

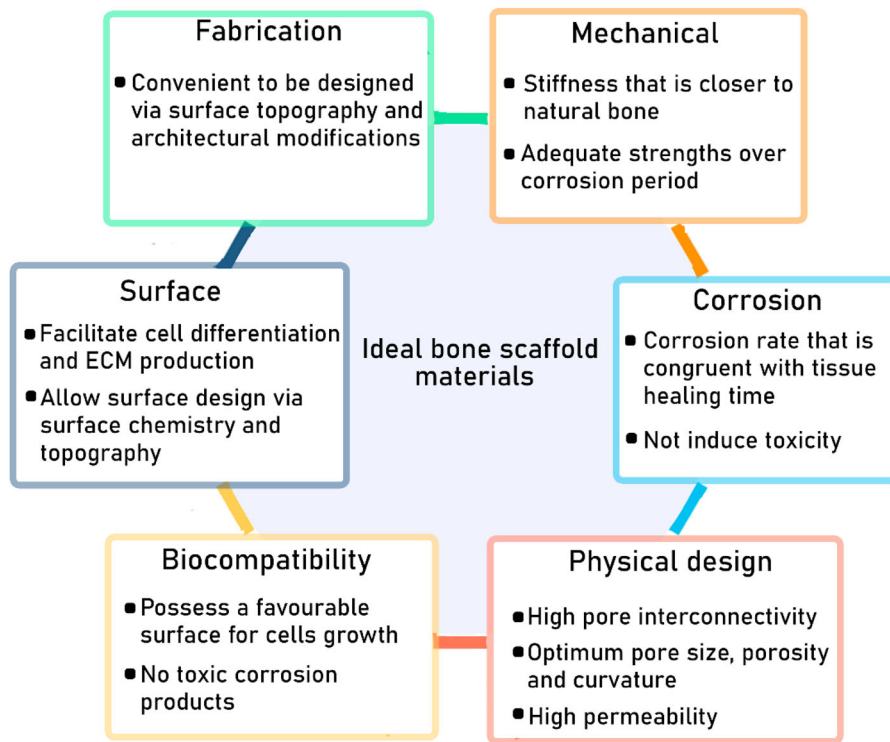


Figure 1. The characteristics of an ideal bone scaffold.

bone, which reduces the concern on the stress-shielding effect [9].

Previous studies have shown that Mg and Mg-based alloys can degrade through corrosion, which emanates from its standard electrode potential of -2.372 V versus normal hydrogen electrode. It has been known that the corrosion of Mg-based implants led to an increase in alkalinity and the release of H_2 gas [10] due to its swift corrosion rate. Many attempts have been performed to resist its rapid corrosion encompassing alloying [11–14], porosity controls [15,16], composite making [17] and surface modifications [18–20]. Song [21] showed that H_2 release rate of 0.01 ml cm^{-2} day^{-1} is harmless and tolerable by the body. Although H_2 gas is non-toxic, if produced excessively, it can lead to local tissue displacement [22], decline of rats' survival rate [23] and deterioration of the mechanical integrity [24,25]. Yazdimamaghani et al. [26] reported that the uncoated porous Mg scaffolds were degraded entirely after 48 h of immersion while polycaprolactone (PCL)-coated porous Mg scaffolds still possessed 10–14 MPa compressive strengths. In short, it can be concluded that the degree of strength deterioration may be exacerbated if H_2 gas is produced in excess and the Mg-based scaffolds present in a highly porous structure.

Various methods to fabricate porous Mg scaffolds have been used, including powder metallurgy (PM) with space holder, infiltration casting, freeze casting, computer numerical control (CNC) drilling and laser perforation. Nevertheless, it is challenging to produce fully interconnected porous structures through these techniques, particularly when complex external design and intricate internal architectures are all desired. Thus, this drives the advent of AM technique to fabricate porous Mg-based scaffolds with precise control of the architecture. This has led to the increasing number of studies performed recently to understand the relationship between topological features of scaffolds and

their mechanical properties, biocorrosion and cell–materials interaction [27–30].

Li et al. [28] used selective laser melting (SLM) technique to produce topologically ordered porous Mg WE43 alloys scaffolds. Based on the finding shown in Figure 2, they suggested that the scaffolds experienced uniform corrosion at the periphery and a localised corrosion in the centre. Despite this new finding, the degree to which it affects the overall corrosion rate of the AM WE43 alloys is still unknown. Bear in mind that the localised corrosion may trigger the formation of cracks on the metallic struts. Table 1 summarises corrosion data of porous Mg-based scaffolds with their corresponding properties and fabrication methods.

Fe corrosion behaviour

Iron (Fe) is an important trace element that plays vital roles in the human body, including cell growth, transport and storage of oxygen, and reduction of RNA and DNA [43]. Since Fe was explored as a potential absorbable metal at the start of the twenty-first century by Peuster et al. [44] via an *in vivo* study for coronary stent applications, Fe-based implants have been intensively studied both *in vitro* and *in vivo* environments to unravel its potential and properties aimed for temporary medical implantations.

While Mg is lightweight and possesses appropriate mechanical strength as an implant material [9], Fe materials are proven to have better mechanical properties than Mg. The comparison between these pure metals is presented in Table 2. One of the primary advantages of Fe materials over Mg is their superior mechanical strengths making it a suitable candidate for implants which require a high structural strength. Besides, Fe also offers excellent ductility and formability.

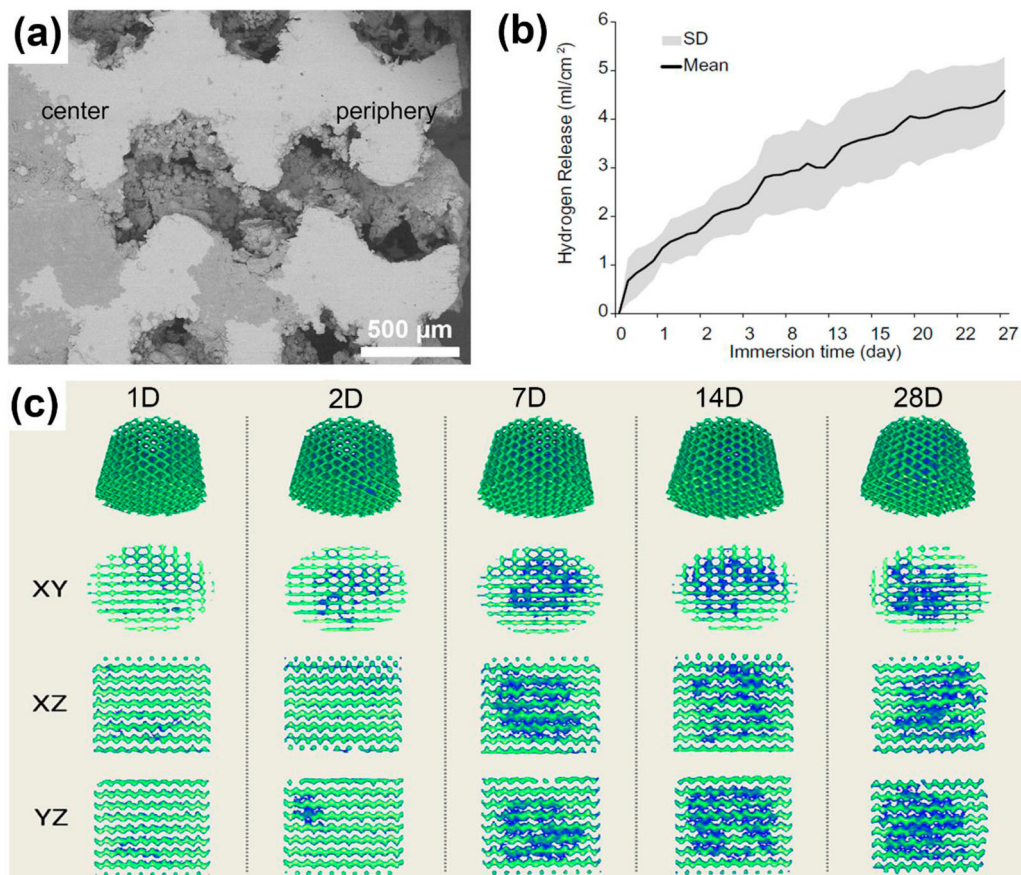


Figure 2. Corrosion findings from AM porous Mg alloys (WE43); (a) Backscattered electron (BSE) image of degradation at the centre of the WE43 scaffolds, (b) hydrogen release and (c) 3D reconstruction of the degraded scaffolds over corrosion period obtained from micro-CT analysis.

Important for cell functions, about 8–27 mg Fe is required by the human body daily [45]. Electrochemically, Fe corrodes in a physiological environment producing Fe^{2+} ions [46] which then react with OH^- ions from oxygen (O_2) reduction to form $\text{Fe}(\text{OH})_2$. The OH^- ions could increase the local pH [47,48] and the compounds such as $\text{Fe}(\text{OH})_3$, FeCO_3 or Fe-phosphates may produce which could precipitate on the Fe surface and in turn impeding the O_2 transport onto the Fe surface [49]. The corrosion rate of Fe in physiological environments is considered excessively slow for bioresorbable applications [50]. In fact, Fe has the lowest standard electrode potential of -0.44 V when compared with those of Mg (i.e. -2.372 V) and Zn (i.e. -0.76 V) versus normal hydrogen electrode, implying its slowest corrosion kinetics among the three members of absorbable metals members. The extremely low solubility of Fe-based corrosion products which could act as a dense protective layer hinder O_2 diffusion to the Fe surface and thus decelerating the redox reactions.

Till present, a variety of methods have been attempted to ameliorate the corrosion rate of Fe-based scaffolds such as alloying [51–53], surface coatings [47,54–57] and porosity control [58]. Topologically ordered porous Fe scaffolds with controllable porosity, pore size and architecture have been produced through AM fabrication methods such as SLM method, inkjet 3D printing and binder-jetting 3D printing [48,53,59–63]. The AM porous Fe-based scaffolds fabricated with various types of unit cells, pore size and porosity are shown in Figure 3. Li et al. [64] demonstrated that the specific solidification process during the AM process could produce porous Fe with smaller grain size, thus

increasing the grain boundary area with defects in the crystal structure and high internal energy. The large grain boundary areas are expected to be more chemically active in a corrosive medium [65]. This will lead to a higher corrosion rate of the porous Fe scaffolds produced.

One of the most recent developments on porous Fe-based scaffolds is the advent of dynamic-flow corrosion as a new corrosion testing condition. Recently, Li et al. found that the corrosion prominently took place both at the periphery (Figure 4(a)) and in the centre (Figure 4(b)) of the porous Fe in the dynamic immersion [64] while in the static immersion, the struts in the centre (Figure 4(d)) remained almost intact [59]. They related this to the fluid flow in the dynamic-flow immersion. However, based on our review, we observed that the overall corrosion rate has not expedited much in the dynamic corrosion, possibly owing to the formation of dense Fe-based oxides products which could counteract the dynamic effect. Table 3 summarises corrosion data of porous Fe-based scaffolds with their corresponding properties and fabrication methods.

Corrosion–porosity relationship

The corrosion rate of porous Mg-based and Fe-based scaffolds in the function of porosity is summarised in Figure 5. Apparently, porous Mg-based scaffolds show a relatively higher corrosion rates (0.04 – 7.92 mm year $^{-1}$) than porous Fe-based scaffolds counterparts. A noticeable change in corrosion rate was observed when subjected to the dynamic immersion as the corrosion rates escalate to 4.62 – 7.41 mm year $^{-1}$. Rapid corrosion of Mg, especially in its porous

Table 1. Corrosion rate data of porous Mg-based scaffolds with their corresponding fabrication methods, corrosion rates and porosity.

Materials	Fabrication methods	Corrosion medium	Corrosion rate				Porosity	
			Electrochemical (mm year ⁻¹)	Static immersion (mm year ⁻¹)	Dynamic immersion (mm year ⁻¹)	Hydrogen evolution (mm year ⁻¹)	Total porosity (%)	Pore size (μm)
Porous Mg alloys [31]	PM	0.9% NaCl	3.5	–	–	–	17 ^a	–
Porous Mg alloys [31]	PM	PBS	7.4	–	–	–	17 ^a	–
Porous Mg–Zn [17]	PM	SBF	3.3–3.9 × 10 ⁻³ A cm ⁻²	–	–	–	21–23	200–400
Porous Mg alloys (EW10X04) coated with Nd [20]	CNC drilling	DMEM	–	0.6–1.3	–	–	25	1000
Porous Mg alloys (EW10X04) [20]	CNC drilling	DMEM	–	1–1.8	–	–	25	1000
Porous Mg [32]	CNC drilling	SBF	–	–	4.9–7.0	0.45–1.14	30–55	800
Porous Mg coated with MgF ₂ [33]	Titanium wire space holder (TWSH)	DMEM	–	1.31–1.53	–	–	54	243 387
Porous Mg [34]	CNC drilling	SBF	–	–	4.9–11.2	–	30–55	800
Porous Mg [16]	CNC drilling	SBF	–	–	5.8–9.6 ^b	–	30–55	800
Porous Mg–Nd–Zn alloys [12]	Titanium wire space holder (TWSH)	DMEM with 10% FBS	–	0.83	–	–	–	200
Porous WE43 alloys [12]	Titanium wire space holder (TWSH)	DMEM with 10% FBS	–	1.73	–	–	–	200
Porous AZ31 Mg coated with MgF ₂ [10]	Laser perforation	Hank's	–	1.18	–	–	–	300
Porous AZ31 alloys [10]	Laser perforation	Hank's	–	1.94	–	–	–	300
Porous Mg–Zn–Ca alloys [14]	PM	Hank's	1.01–2.86	–	–	–	–	–
Porous Mg–Zn coated with nano HA [35]	PM	SBF	1.47	–	–	–	23	–
Porous Mg–Ca–Zn–Co [36]	PM	SBF	1.11–5.93	–	–	–	74	400–890
Porous Mg–Ca–Zn–Co [11]	PM	SBF	–	2.28	–	–	74	–
Porous Mg [15]	Infiltration casting	DMEM + 10%FBS	–	0.52– 4.36	–	–	68–75	750
Porous Mg–Ca–TiO ₂ [37]	PM	SBF	210.7 μA cm ⁻²	–	–	–	65–67	600–800
Porous Mg alloys (WE43) [28]	Selective laser melting (SLM)	r-SBF + 5% FBS	1.04	–	–	–	64	–
Porous Mg coated by HA/(PEI–15% SiO ₂) [19]	PM + spark plasma sintering (SPS)	SBF	–	–	–	0.7	70	220
Porous Mg–Al alloys [13]	Freeze-casting	E-MEM + 10% FBS	951 μA cm ⁻²	–	–	–	52	10–100
Porous Mg alloys (WE43) [27]	Selective laser melting (SLM)	r-SBF	–	7.92 ^b	–	–	65.5	417
Porous Mg [38]	CNC drilling	SBF	–	–	6.3–6.7	–	30–55	800
Porous Mg/Si ₃ N ₄ [39]	Microwave sintering	SBF	1.36 × 10 ⁻³ A cm ⁻²	–	–	–	45.7	–
Porous Mg/Al ₂ O ₃ [39]	Microwave sintering	SBF	5.53 × 10 ⁻³ A cm ⁻²	–	–	–	52.9	–
Porous Mg–10Zn–4Y alloys [40]	PM and space holder	PBS	–	0.13	–	–	50	300
Porous Mg coated by MgF ₂ [41]	PM and space holder	PBS	–	0.003 g day ⁻¹	–	–	60	400–600
Porous Mg–6Zn alloys [42]	PM and space holder	Hank's	–	6.5–37.4 mg cm ⁻² day ⁻¹	–	–	6.7–52.5	32.3–384.2

Note: All the corrosion rates data are in mm year⁻¹ unit, unless stated otherwise.

^aOpen porosity.

^bUnder cyclic loading.

structure, is further accelerated due to the fluid flow. These high corrosion rates signify the severity of the corrosion experienced by porous Mg in the dynamic condition as it integrates the environment of fluid movement passing through cancellous bone.

AM porous WE43 alloys exhibited a satisfactory corrosion rate of 1.04 mm year⁻¹ after 4 weeks immersion despite its very large surface area (i.e. 25.4 cm²). Li et al.

[28] related this satisfactory corrosion rate to the large grain boundaries from finer microstructure which acted as a corrosion barrier and could reduce the intensity of micro galvanic corrosion. However, its corrosion rate substantially jumped to 7.92 mm year⁻¹ after being subjected to cyclic loading [27]. From our perspective, it is hard for the porous Mg-based scaffolds to achieve a slower and satisfactory corrosion rate without any modifications such as surface coating

Table 2. Mechanical properties of pure Fe and Mg.

Metals	Tensile strengths (MPa)	Yield strength (MPa)	Maximum elongation (%)
Fe-based: Young's modulus ~ 200 GPa, density ~ 7.8 g cm ⁻³			
Pure Fe (annealed)	150	200	40
Mg-based: Young's modulus ~ 45 GPa, density ~ 1.7 g cm ⁻³			
Pure Mg (extruded)	30	100	7

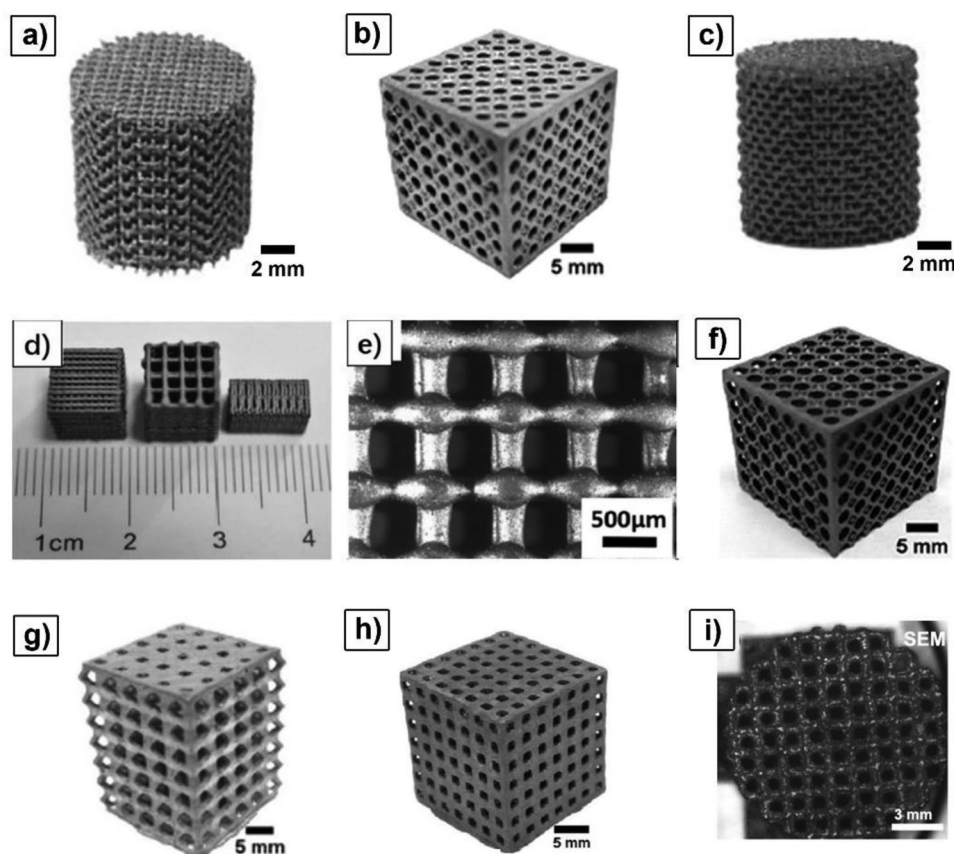
or porosity control. As shown by its rapid corrosion rates in dynamic flow, the modifications on the porous Mg appear necessary to avoid the negative effects resulting from the excessive corrosion.

One of the distinct findings here is that most of porous Fe-based scaffolds were produced at higher porosity (>80%), while porous Mg-based scaffolds have been prepared in the range of 17–76% porosity. Higher strengths of pure Fe could compensate for the higher porosity produced to ensure the strengths of the porous Fe scaffolds are within the ranges of those of cancellous bone. Although being produced in a higher porosity, the corrosion rates of porous Fe-based scaffolds do not surpass those of porous Mg-based scaffolds which are produced at a relatively lower porosity. This can be explained by Fe's standard electrode potential which is far lower than that of pure Mg.

Aside from that, the corrosion rate data also reveal that the unmodified bare porous pure Fe scaffolds have higher corrosion rates (0.03–2.25 mm year⁻¹) compared to that of reported bare non-porous bulk pure Fe counterpart (0.008–0.242 mm year⁻¹) electrochemically [4,77–83]. This

signifies the benefit of porous structure in expediting Fe's too-slow corrosion kinetics. Further, the AM design of porous Fe has a minimal impact on the escalation of the corrosion rate as some of the AM Fe possess a higher corrosion rate (1.18–2.25 mm year⁻¹) than non-AM Fe even produced at a relatively lower porosity (73–84%) implying the advantage of larger exposed surface area of the AM design. Grain refinement following the high cooling rate in AM techniques could also attribute to this increment due to the increased amount of grain boundaries [59,84]. Higher surface reactivity to corrosion is also expected due to the high cooling rate during the AM process [85]. Nevertheless, there are some discrepant cases in which some of the corrosion rates of AM porous Fe-based scaffolds (i.e. 0.27–0.85 mm year⁻¹) [64,74] are more or less in the same range of some of unmodified non-AM porous pure Fe scaffolds (0.03–0.75 mm year⁻¹) [51,54,68,70,71] at nearly similar porosity (i.e. 81–89%). Despite having a high pore interconnectivity and permeability besides grain refinement factor which favour accelerated corrosion, we postulate that the passivated surface made up of common dense corrosion products on Fe surface could counteract these topological design and AM factors leading to the mild corrosion kinetics.

Meanwhile, unlike porous Mg-based scaffolds, it has been observed that the dynamic immersion does not influence the corrosion rates of porous Fe-based scaffolds much thus far. In addition, it can be deduced that there was only little impact of dynamic immersion observed on the corrosion rates of AM porous Fe scaffolds in comparison to static immersion. After 28 days of the corrosion period, the dynamic immersion scaffolds showed a satisfactory corrosion rate of 1.24 mm year⁻¹ [64], while similar types of

**Figure 3.** The AM porous Fe-based scaffolds fabricated with various types of unit cells, pore size and porosity [48,59,60,62,66,67].

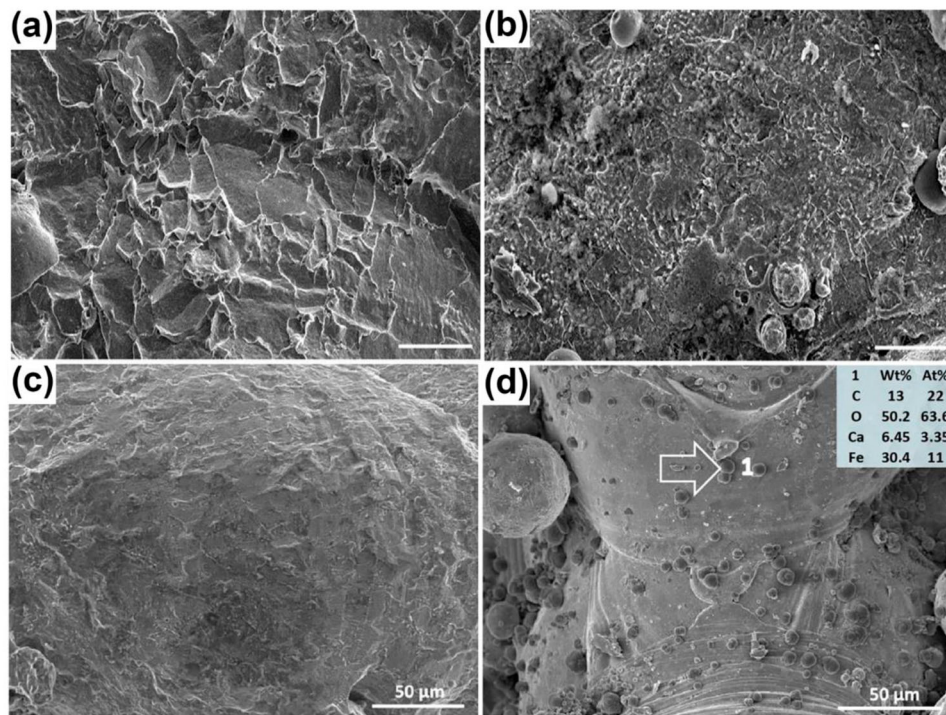


Figure 4. Morphologies of the degraded AM porous Fe scaffolds after cleaning on the (a) periphery and (b) in the centre in dynamic-flow corrosion, (c) periphery and (d) in the centre in static immersion [59,64].

AM porous Fe had $1.18 \text{ mm year}^{-1}$ corrosion rate in static immersion [59]. The dynamic flow renders the fresh Fe surface to be exposed to the media and this supposedly enhanced its corrosion rate. However, we postulate that the extremely slow anodic reaction kinetics of Fe (i.e. substrate dissolution rate) allows the formation of corrosion products to counteract the advantage of fresh surface exposure. This might lead to the mild increase in corrosion rate in dynamic immersion in comparison to that of static immersion.

Comparing the corrosion rate value at almost similar porosity and fluid flow rate, the AM porous Fe having 58% porosity showed $0.27 \text{ mm year}^{-1}$ after 28 days of dynamic immersion executed at 0.3 mL min^{-1} flow rate. Conversely, porous Mg with 55% porosity developed by Md Saad et al. [34] demonstrated $8.39 \text{ mm year}^{-1}$ corrosion rate only after 3 days of dynamic immersion at 0.4 mL min^{-1} flow rate. This obvious difference is inherent to the rapid nature of Mg corrosion characteristic when compared with the much slower rate of Fe, which is further exaggerated when stimulated by fluid flow environment. From our view, the flowing SBF could swiftly remove the corrosion products on the porous Mg surface and renders the fresh Mg surface to be exposed to the media. Owing to Mg rapid corrosion kinetics, this will accelerate anodic reaction of Mg dissolution leading to the high corrosion rate. However, this is not exactly the case for porous Fe-based scaffolds. As the fresh Fe surfaces exposed to the media, its much slower substrate dissolution rate renders the formation of corrosion products to counteract the advantageous effect of fresh surface exposure. This leads to the much lower corrosion rate of porous Fe even in dynamic immersion. In other words, porous Mg with its rapid dissolution rate seems to take a full advantage of the fresh substrate exposure from the dynamic fluid flow across it while this advantage is partly impeded for porous Fe due to their slower anodic reaction.

Figure 6 summarises the elastic modulus of porous absorbable metals with respect to their corrosion rates. An ideal bone scaffold should have an elastic modulus which is closer to that of natural bone (0.01–20 GPa) [86]. Referring to the figure, the dynamic immersion apparently led to the diminishing of the elasticity of porous Mg scaffolds and to the acceleration of the corrosion rate despite their lower as-fabricated porosity when compared with and Fe-based counterparts.

The production of porous Fe-based scaffolds in a higher porosity (>80%) considerably deteriorates its elastic modulus to 0.003–0.2 GPa, even though the porosity is in the range of cancellous bone's porosity (40–90%) [86]. Higher porosity can facilitate tissue growth but at the expense of losing elasticity. Further, the fabrication of porous Fe in topologically ordered design mildly enhances the elasticity. The AM techniques namely direct metal printing (DMP) and SLM used to fabricate the topologically ordered porous Fe led to grain refinement due to the high cooling rate and rapid solidification following high energy powder melting which give rise on the strengths [64,85]. Nevertheless, this AM effect may be overshadowed by the porosity factor as all the AM porous Fe have a relatively lower porosity (58%, 77% and 84%) than most of non-AM porous Fe-based scaffolds which possess more than 88% porosity.

In comparison, porous Fe-based scaffolds with 77% and 58% porosity show elastic modulus of 1.6 and 2 GPa when subjected to 24 h static and 28 days dynamic immersions, reducing about 9% and 27% of their initial as-fabricated elasticity, respectively [59,64]. Nevertheless, the post-corrosion elasticity is in a high range of cancellous bone elasticity (0.01–2 GPa). Porous Mg-based scaffolds with 30% and 41% porosity show 41% (from 2.2 to 1.3 GPa) and 66% (from 2.1 to 0.7 GPa) reduction in elasticity, respectively, only after 3 days of dynamic immersions [32]. The above findings showed that despite being produced in a relatively

Table 3. Corrosion rate data of porous Fe scaffolds with their corresponding fabrication methods, corrosion rates and porosity.

Materials	Fabrication methods	Corrosion medium	Corrosion rate				Total porosity (%)	Porosity Pore size (µm)
			Electrochemical (mm year ⁻¹)	Static immersion (mm year ⁻¹)	Dynamic immersion	Hydrogen evolution (mm year ⁻¹)		
Porous Fe coated with HA [68]	Polymer space holder	SBF	0.003	–	–	–	88	450
Porous Fe	Polymer space holder	SBF	0.031	–	–	–	88	450
Porous Fe infiltrated with PLGA [69]	Polymer space holder	PBS	0.72	–	–	–	88	450
Porous Fe [69]	Polymer space holder	PBS	0.11	0.33	–	–	88	450
Porous Fe–Mn–1Ca alloys [53]	3D printing	DMEM	0.07	0.14	–	–	52 ^a	5
Porous Fe–Mn alloys [53]	3D printing	SBF	0.04	0.03	–	–	39 ^a	5
Porous Fe [70]	Electroplating pure Fe on a PU template	Hank's	–	0.29	–	–	89	800
Fe coated with tungsten (W) [70]	Electroplating pure Fe on a template	Hank's	–	0.42	–	–	94	800
Porous Fe–CNT [71]	PM	Hank's	0.67	–	–	–	–	800
Porous Fe–Mg [71]	PM	Hank's	0.97	–	–	–	–	800
Porous Fe [71]	PM	Hank's	0.75	–	–	–	–	800
Porous Fe [51]	Polymer replications and infiltration casting	Hank's	0.44	–	–	–	89	300–800
Porous Fe–P alloys [51]	Polymer replications and infiltration casting	Hank's	0.27–0.38	–	–	–	88–89	250–700
Porous Fe [54]	Polymer replications and infiltration casting	Hanks	0.31	–	–	–	89–93	300–800
Porous Fe coated with PLA/HA [54]	Polymer replications and infiltration casting	Hank's	0.48	–	–	–	80–85	300–800
Porous Fe–30Mn6Si1Pd alloys [72]	PM	Hank's	0.48	–	–	–	62.3	8
Porous Fe [73]	Polymer space holder	Modified Hanks'	87.8 µA cm ⁻²	–	–	–	90	818
Porous Fe coated with CaP/Ag [73]	Polymer space holder	Modified Hanks'	8.4–10.9 µA cm ⁻²	–	–	–	90	818
Porous Fe [59]	Additive manufacturing-Direct metal printing (DMP)	Revised SBF	1.18	–	–	–	73	749
Pure Fe [47]	Polymer space holder	PBS	0.23	–	–	–	88	450
Porous Fe coated with curcumin/PLGA [47]	Polymer space holder	PBS	0.37–0.98	–	–	–	88	450
Porous Fe–30 Mn [58]	Space holder method and PM	α-MEM	0.14–0.98	0.13–0.38	–	–	15–32	–
Porous Fe [64]	Selective laser melting (SLM)	Revised SBF	–	–	0.27–1.24	–	58–84	506–755
Porous Fe [62]	SLM	Revised SBF	–	0.023–0.148 ^b	–	–	73	–
Porous Fe [74]	3D printing and microwave sintering	SBF	0.85–2.25	–	–	–	45–81	1170–1580
Porous Fe [75]	3D printing and microwave sintering	SBF	0.62–1.64	–	–	–	45–87	–
Porous Fe–25Mn [66]	SLMSLM	SBFHank's	–0.8	0.23	–	–	66.742.6	–400
Porous Fe–35Mn [76]								

high elastic modulus and with a low porosity, porous Mg-based scaffolds encountered a substantial reduction in elasticity even after a few days of corrosion periods. Yazdimaghani et al. [26,87] reported that the uncoated porous Mg scaffolds were degraded almost entirely after 48 and 96 h of immersions in a series of corrosion study.

In contrast, porous Fe-based scaffolds which have a relatively higher initial porosity experienced a low reduction in elasticity even after a more extended corrosion period. From our view, the aforementioned significant trend is mainly ascribed to the rapid corrosion pace of porous Mg-based scaffolds when compared with the much slower rates of porous Fe. The swift corrosion of Mg will lead to an intense Mg dissolution which catalyses the Mg weight loss. This will deteriorate the strength retention much resulting into a substantial strength loss. Conversely, the relatively lower post-corrosion elasticity of porous Fe-based scaffolds

is mainly due to the high fabrication porosity (>85%) considering that too-slow corrosion pace of these scaffolds will not considerably diminish the strengths. Thus, we can recapitulate here that the strength retention of porous Fe-based scaffolds is much higher than that of porous Mg-based scaffolds in the corrosion environment.

As indicated in Figure 7, Zheng et al. [6] suggested that the mechanical support should be sustained for 12–24 weeks depending on the fracture configuration and location, status of the adjacent soft tissues and patient characteristics (e.g. species, age, health status, concurrent injuries/diseases). Other reports also suggested that the load-bearing orthopaedic implants should maintain mechanical integrity over a timescale of 12–18 weeks while the bone tissue heals [8,88]. We expect that these time frames could be difficult to be achieved by porous Mg-based scaffolds as they could substantially lose mechanical integrity only within few days of

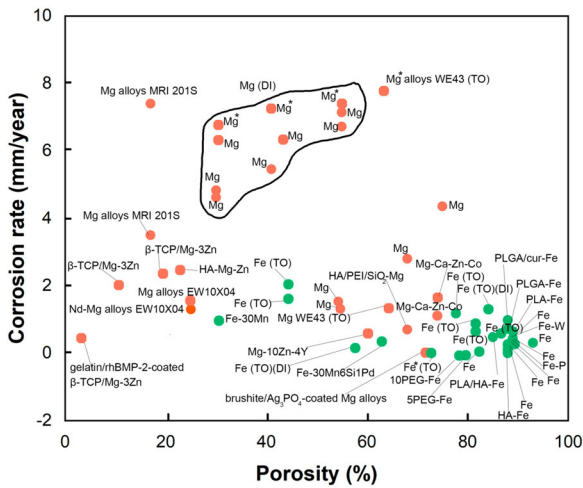


Figure 5. Corrosion rate of porous Mg and Fe in function of porosity. The corrosion rate data are obtained from all methods (electrochemical technique, static and dynamic immersion) and are normalised to mm/year unit. (TO corresponds to topologically ordered porous scaffolds, DI refers to dynamic immersion and * represent scaffolds subjected to cyclic loading.)

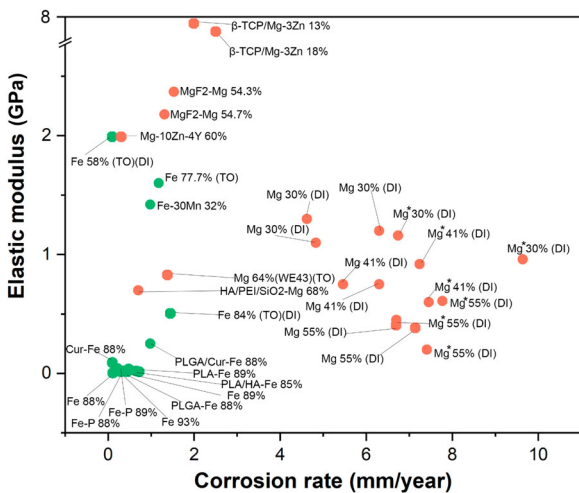


Figure 6. Elastic modulus of porous Mg-based and Fe-based scaffolds in the function of corrosion rate. The corrosion rate data are obtained from all methods (electrochemical technique, static and dynamic immersion) and are normalised to mm/year unit. (TO refers to topologically ordered porous scaffolds, DI indicates dynamic immersion and * refers to scaffolds subjected to cyclic loading).

immersion [16,32,87]. On the contrary, the slow corrosion kinetics of porous Fe-based scaffolds could favour this requirement as recent reports indicated that their mechanical

strengths reduced minimally even after 28 days of corrosion period [47,89].

The cell viability of porous Mg-based scaffolds in the function of corrosion rate is summarised in Figure 8. It can be seen that most of the modified porous Mg-based scaffolds have 70% or higher viability after certain corrosion periods signifying the positive effect provided by the modifications on the porous Mg including surface coating, alloying and composite making. Some of them are able to retain the good cell viability even after 4 and 7 days of cultivation [33,90]. These findings are further supported by the viability results of porous modified Mg-based scaffolds without corrosion rate and viability data, when compared with those of unmodified porous Mg scaffolds, as shown in Table 4. Furthermore, the data also reveal that the lowest two viability is shown by the unmodified bare porous Mg-based scaffolds and this finding may imply the significant impact of modifications on porous Mg-based scaffolds in enhancing their cell viability.

Even though the cell viability might differ due to the different cell lines used, different corrosion periods and extract concentrations, and medium, the vast reports on the positive effect of Mg ions on tissue growth including those of bulk Mg-based implants support these aforementioned findings. Zhang et al. [91] concluded that the culture medium environment containing Mg ions is beneficial to cell proliferation and on that account, the developed porous Mg-Zn-Ca alloys scaffolds exhibited high osteoblast adhesion and proliferation. Liu et al. [12] found that the suitable concentration of Mg^{2+} and Zn^{2+} in medium may contribute to better proliferation and osteogenic differentiation of porous Mg-Nd Zn scaffolds, on top of enhanced corrosion resistance factor.

AM porous WE43 scaffolds exhibited a good cell viability in overall despite the 24 h WE43 extracts revealed cytotoxicity level 1. Li et al. [28] concluded that the finer grain produced from the AM technique, passive layer formation and the protein-containing medium altogether attribute to a satisfactory corrosion rate which, in turn, leading to an appropriate concentration of released Mg^{2+} . This delicate release of Mg^{2+} provided a favourable environment for the cell growth. Note that the recommended daily intake (RDI) is suggested to be a key measure for assessing a material's biocompatibility. In fact, the adult's RDI of Mg (375–700 mg) is much higher than those of Fe (10–20 mg) and Zn (6.5–15 mg) and this offers Mg with a high tolerance once implanted in the human body. This RDI could indicate the higher

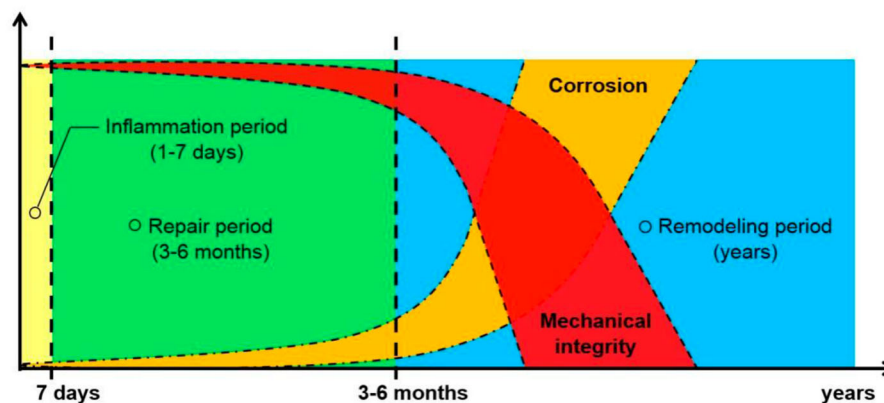


Figure 7. Illustration of the ideal compromise between mechanical integrity and corrosion of absorbable metals for bone implant [6].

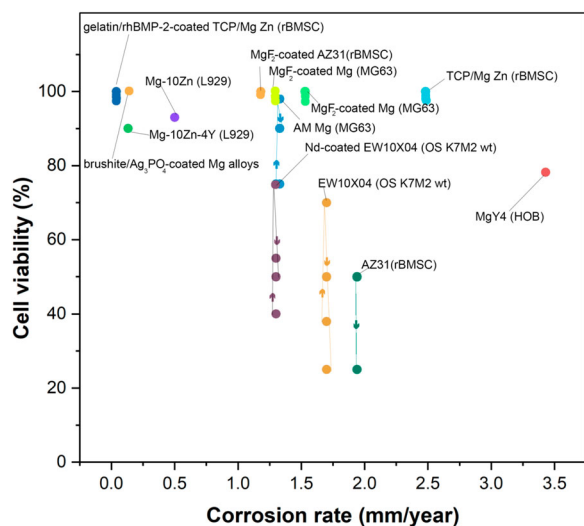


Figure 8. Cell viability of porous Mg-based scaffolds in the function of corrosion rate. Arrows indicate the changes in the cell viability.

biocompatibility of Mg-based scaffolds when compared with those Fe-based scaffolds.

Unfortunately, porous Mg is not without its issues. An *in vitro* study by Yazdimamaghani et al. [18] indicated that the rapid corrosion and swift H_2 evolution of porous Mg scaffolds affected the cell adhesion. Yu et al. speculated that the high osmotic pressure generated from the high concentration of Mg^{2+} from porous AZ31 alloys reduced the viability of the rBMSC. Further, they found that poor cell proliferation and bone resorption might be due to local high concentration of Mg^{2+} and high alkalinity from the continuous excessive corrosion [10]. In this regard, despite vast reports indicating positive effects of Mg ions on bone cells, their corrosion products such as Mg-based oxides products and H_2 evolution should be controlled so as not to incite cytotoxicity in the static *in vitro* test. Considering the nature of the static and stagnant flow of the *in vitro* test condition which involve no dynamic electrolyte flow, we anticipate that the intensity of the H_2 evolution could be high in the system which could render cytotoxicity and this phenomenon could be exacerbated due to the highly rapid corrosion pace of the Mg scaffolds.

Figure 9 shows the cell viability of porous Fe-based scaffolds with respect to their corrosion rates. One of the important findings here is the reduction of cell viability throughout the whole range of the corrosion rate. Accordingly, porous Fe scaffolds with high or low corrosion rates could experience the declination of the cell viability. Of note, based on the data presented in Figure 9 and Table 4, only several studies reported the acceptable viability or cytotoxicity level 0 (75%–99%) of unmodified bare porous Fe-based scaffolds at an extended incubation period as the viability usually deteriorated after 24 h incubation [48,69]. Very recently, topologically ordered porous Fe scaffolds showed more than 90% cell viability after 1-day incubation, but it deteriorates after 3 days incubation and some of the scaffold groups exhibited cytotoxicity level 2 (<50%) [48]. The similar diminishing trend was reported by other studies as well [64,70,71].

Some studies reported an improved viability of porous Fe-based scaffolds after undergoing modifications such as surface coating, alloying and composite making after a longer

time period [53,67,69,70]. As can be seen from Figure 9 and Table 4, producing AM porous Fe with topologically ordered structural design did not contribute to the enhancement of cell viability as all three studies reported the significant decrease of the viability after a longer corrosion period due to the high accumulation of Fe ions [48,64,89]. These AM recent findings imply that the potential cytotoxicity of Fe-based scaffolds even being fabricated with a high pore interconnectivity. Accordingly, we opine that the adverse effect of Fe corrosion products seems to surpass and decline the advantage of uniform porous structure, high permeability and excellent pore interconnectivity of AM scaffolds in enhancing the cell growth.

Based on the discussed findings, the cytotoxicity of Fe-based scaffolds could emerge due to two main factors, namely the excessive release of Fe^{2+} and the accumulation of insoluble Fe-based oxide corrosion products [48,54,59,64,68,70,71,92]. Additionally, the Fe^{2+} which is free to participate in Fenton chemistry could generate hydroxyl free-radicals formation and then leading to the oxidative stress in the media [93,94].

Apart from that, we believe that the low bioabsorption of low-soluble oxides such as Fe_2O_3 and Fe_3O_4 could attribute to this low biocompatibility due to the possible induced toxicity. The hardly dissolved corrosion products will remain in insoluble state for a certain time period and these insoluble corrosion products have been shown to incite cytotoxicity [52,95].

In this respect, excessive Fe^{2+} release should be controlled and the formation of insoluble oxide products needs to be reduced as well. This scenario offers a wide range of research opportunities in ensuring produced corrosion products do not exceed the tolerable limit. It has been suggested that a lower Fe concentration (i.e. $<10 \mu g mL^{-1}$) may produce the favourable effect on the metabolic activity of endothelial cells (ECs) while a very high Fe ion concentration (i.e. $>50 \mu g mL^{-1}$) could remarkably reduce it regardless of incubation time [96]. Zhang et al. [97] suggested that Fe ion which is lower than $75 \mu g mL^{-1}$ may prevent cytotoxicity on mouse bone marrow stem cells. Fagali et al. [95] concluded that low levels of soluble Fe ($\approx 15\text{--}30 \mu g$) together with precipitates yielded to reactive species (RS) production. All of these limits could be a benchmark to design a porous Fe-based scaffold without a cytotoxicity potential throughout the corrosion period.

Concluding remarks and perspective

The need of modifications

Based on the earlier discussion, the modifications on porous Mg-based and Fe-based scaffolds are necessary to ameliorate the properties of the scaffolds. Porous Mg-based scaffolds are mainly modified by surface coating to slow down its excessive corrosion and enhancing strength retention and biocompatibility while porous Fe-based scaffolds undergo surface coating and alloying to accelerate its corrosion pace and to augment its biocompatibility. From our standpoint, while the surface coating could enhance the biocompatibility in a short-term corrosion period, this approach is hard to escalate the corrosion kinetic of the Fe-based scaffolds due to the protective nature of the coating materials. The coating will not last longer since it only develops physical interfacial

Table 4. Summary of *in vitro* biocompatibility test of porous Mg-based and Fe-based scaffolds.

Porous scaffolds	Methods	Cells	Significant outcomes
Mg coated by Enoxacin-loaded PLGA [98]	Direct method	Mouse embryo fibroblast (3T3 cells)	The proliferation on the porous Enox-PLGA-Mg samples increased compared to porous pure Mg. PLGA could neutralise the alkaline products of Mg degradation
Mg coated with polymer/hydrogel/ceramic composite layer [18]	Direct method	Human osteosarcoma cells (Saos-2)	The uncoated Mg scaffolds showed rapid degradation which affected the cell proliferation. The corrosion resistance provided by the coating led to a better biocompatibility
Mg/Al ₂ O ₃ coated by MgF ₂ -coated [99]	Direct method	Murine pre-osteoblastic cells (MC3T3-E1)	Relatively more cells were attached to the MgF ₂ -coated surface compared to uncoated samples. The dense MgF ₂ coating on the Mg/Al ₂ O ₃ composites decreased the corrosion rates
AZ31 Mg alloys coated by MgF ₂ [10]	Direct method, extraction medium culture	Rat bone marrow-derived mesenchymal stem cells (rBMSCs)	MgF ₂ coating retarded the robust release of Mg ²⁺ which led to good cell growth and 100% confluence after 7 days of culture
AM Porous Mg (WE43) alloys [28]	Extraction medium culture, Direct method	Human MG63 osteoblasts	Only day 1 WE43 extracts revealed level 1 cytotoxicity while all other days' extracts showed cytotoxicity level 0
MgF ₂ -coated porous Mg [33]	Extraction medium culture	Human MG63 osteoblasts	MgF ₂ layer reduced the hydrogen release and toxicity response caused by the initial high corrosion rate of Mg
EW62 (Mg-6%Nd-2%Y-0.5%Zr) alloys [100]	Extraction medium culture, direct method	Osteosarcoma K7M2 wt	The cell viability decreased after 24 h incubation due to the corrosion products and the accumulation of H ₂ gas and increased after 48 h due to effective passive layer on Mg surface
Mg-Nd-Zn (P-MNZ) alloys [12]	Extraction medium culture	Human MG63 osteoblasts	P-MNZ showed a lower cytotoxicity and better proliferation than porous Mg samples due to suitability of Mg ²⁺ and Zn ²⁺ concentrations
Mg-Zn coated by nano HA [101]	Extraction medium culture, direct method	Human MG63 osteosarcoma	The extracts from coated Mg scaffolds with slower corrosion rate improved the cell viability and stimulated the cell proliferation when compared with uncoated Mg scaffolds
Mg-Zn-Ca alloys [91]	Extraction medium culture	Mouse bone marrow stromal cells (BMSC)	The porous alloys scaffolds exhibited higher osteoblast proliferation compared to Ti controls due to the release Mg ions
HA/(PEI-SiO ₂)-coated Mg [102]	Direct method	Murine pre-osteoblastic cells (MC3T3-E1)	The HA/(PEI-SiO ₂)-coated porous Mg had better cell affinities and overall bioactivity than HA-coated porous Mg due to reduced corrosion of porous Mg
AM porous WE43 alloys [28]	Extraction medium culture	MG-63 cells	Only 24 h WE43 extracts revealed cytotoxicity level 1 while all other days' extracts fulfilled cytotoxicity level 0 requirements
Mg10Zn4Y coated with trimethoxysilane [40]	Extraction medium culture	L929 fibroblast cells	The coated porous Mg10Zn4Y exhibited 95% viability while uncoated bulk Mg showed a 90% viability. The coating acted as a protective layer improving the degradation rate
EW10X04 coated with Nd [20]	Extraction medium culture, direct method	Osteosarcoma K7M2 wt	The Nd coating slowed down the corrosion leading to a higher cell viability. Live cells were observed on coated scaffolds at all times
Gelatin/rhBMP-2-coated β-TCP/Mg-Zn composite [90]	Extraction medium culture	rBMSC cells	The coated scaffolds showed a better proliferation after 4 days cultivation. The low immunogenicity and good biocompatibility of gelatin facilitate this favourable effect
Fe, porous Fe-CNT and porous Fe-Mg [71]	Direct method, proliferation by fluorescence microscopy	Murine pre-osteoblastic cells (MC3T3-E1)	All pure Fe, Fe-CNTs and Fe-Mg samples inhibited the cell viability as the osteoblast cell densities decreased after 3 days culture due to the excessive accumulation of degradation products
HA-coated porous Fe [68]	Direct method	Human skin fibroblast cells (HSF 1184) and hMSC cells	The excessive Fe ions lowered the HSF cells viability after day 5. Meanwhile, the surface wettability of HA-Fe could support hMSC cells adhesion
Fe and porous Fe-Mg, Fe-CNT alloys [92]	Direct method	Fibroblast cells	Excessive degradation products resulting from the corrosion process retarded the cells viability of all the tested samples
PLGA-impregnated porous Fe [69]	Direct method	Human skin fibroblast cells (HSF 1184)	PLGA-Fe had higher cell viability compared to bare porous Fe as PLGA surface provided a favourable microenvironment for cell proliferation
Fe coated by Fe-W alloys [70]	Extraction medium culture	Murine pre-osteoblastic cells (MC3T3-E1)	The pure Fe and 1.5FeW scaffolds with the fastest corrosion showed a significant decrease in the cell viability due to the accumulation of Fe ions in the medium
Fe-Mn-Ca/Mg alloys [53]	Direct method, extraction medium culture	Murine osteoblast-like cells (MC3T3)	Fe-Mn-1Ca showed more live cells compared to Fe-Mn or Fe-Mn-Mg samples. The addition of Ca enhanced the biocompatibility of the Fe-Mn alloys
PLA and PLA/HA-coated porous Fe [54]	Direct method	Mouse pre-osteoblastic cells (MC3T3-E1)	The pure Fe and PLA/HA-Fe samples showed no sign of toxicity after 24 h of cultivation. No live cells on pure Fe and PLA/HA-Fe samples after 48 h of cultivation
Fe-Mn-Si-Pd alloys [72]	Direct method, proliferation by fluorescence microscopy	Human osteo Saos-2	The pronounced ion release and poor adhesion of the corrosion oxide layer resulted into progressive decrease of live cells. The ions and debris from the corrosion posed a negative effect on the cells
Nano HA-coated porous Fe [67]	Direct method	Rabbit bone marrow mesenchymal stem cells (rBMSCs)	Cells proliferated well on HA-coated Fe samples compared to uncoated samples. The reduced Fe ion concentration by HA coating resulted to enhanced biocompatibility
Iron oxide nanostructured arrays [103]	Extraction medium culture	Human osteosarcoma cells (MG-63)	The high cell viability of the extract samples indicated that the release of Fe ions concentrations was non-toxic to the MG-63 cells
AM porous Fe [89]	Extraction medium culture, direct method	Human osteosarcoma cells (MG-63)	After 24 h, only a few cells were alive on Fe scaffolds compared to Ti-6Al-4 V scaffolds. High local accumulation of Fe ²⁺ ions could contribute on this low viability
AM porous Fe [64]	Extraction medium culture, direct method	Human osteosarcoma cells (MG-63)	After 24 h, the scaffolds exhibited non-cytotoxic property. Only after 72 h-extractions, the samples showed a moderate cytotoxic (i.e. level 2) due to the oxidative stress in the media

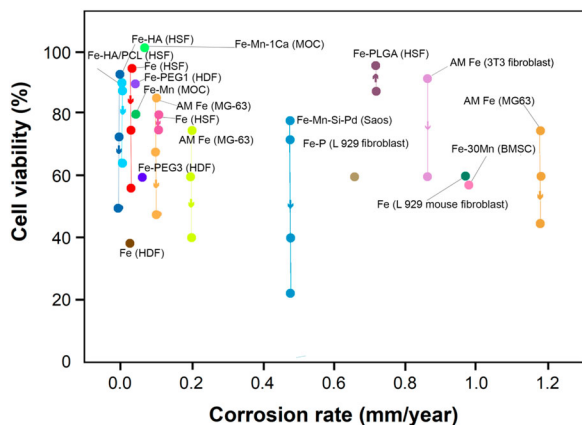


Figure 9. Cell viability of porous Fe-based scaffolds in the function of corrosion rate. Arrows indicate the changes in the cell viability.

interactions in the forms of weak hydrogen bondings or van Der Waals forces with Fe or Mg surface. In addition, due to the hydrophilic characteristic and biodegradable property, some of the coating materials could deteriorate once they react with SBF.

Conversely, alloying provides a longer and continuous corrosion adjustment *in vitro* since it involves microstructural alteration which could provide a longer galvanic corrosion effect. Owing to the presence of alloying element in the solid solution, the corrosion thermodynamic enhancement of the Mg-based and Fe-based alloys could be sustained in a longer time period. Nevertheless, alloying has a higher propensity to decline the biocompatibility owing to the released insoluble corrosion products and ions from the metallic alloying elements as well as to the direct cell-metallic surface interactions. We also postulate that the topologically ordered design has the ability to substantially expedite the corrosion rate for a longer corrosion period *in vitro* due to

the ordered porosity with a very large exposed surface area. Despite all that, it still could incite early cytotoxicity if the AM porous scaffolds do not undergo any modifications due to the direct surface–cells interactions.

Improving porous Mg

While the corrosion rate of most Mg-based implants is faster than is desired for orthopaedic applications, the opposite holds for Fe-based implants. Many attempts have been made to slow down the rapid corrosion of porous Mg since it severely deteriorates the mechanical integrity. Although Mg implants in bulk (non-porous) structure have been clinically studied and even commercialised, commercialising porous Mg scaffolds is a tremendous challenge as it is hard to maintain an adequate mechanical integrity throughout the corrosion period, especially when tested in a dynamic-flow condition, as shown in the elasticity data.

In this regard, further research is needed to improve the mechanical integrity of Mg-based implants. For instance, modifications on porous Mg-based scaffolds are necessary to control its excessive corrosion. While coating could only retain in a short time period and AM design could exacerbate the corrosion pace, alloying seems like a promising approach to enhance its mechanical strength and control the corrosion for a longer period. For an even better outcome, the alloying could be coupled with porosity optimisation and surface coating to further enhance the strength retention as corrosion take its course.

Despite having a rapid corrosion rate, the biocompatibility of Mg-based scaffolds is considered better than those of porous Fe-based scaffolds, attributing to the much higher tolerance and more positive effects of Mg ion on the bone tissues. However, the increase in pH and alkalinity in the surrounding corrosion environment, high H_2 release and even

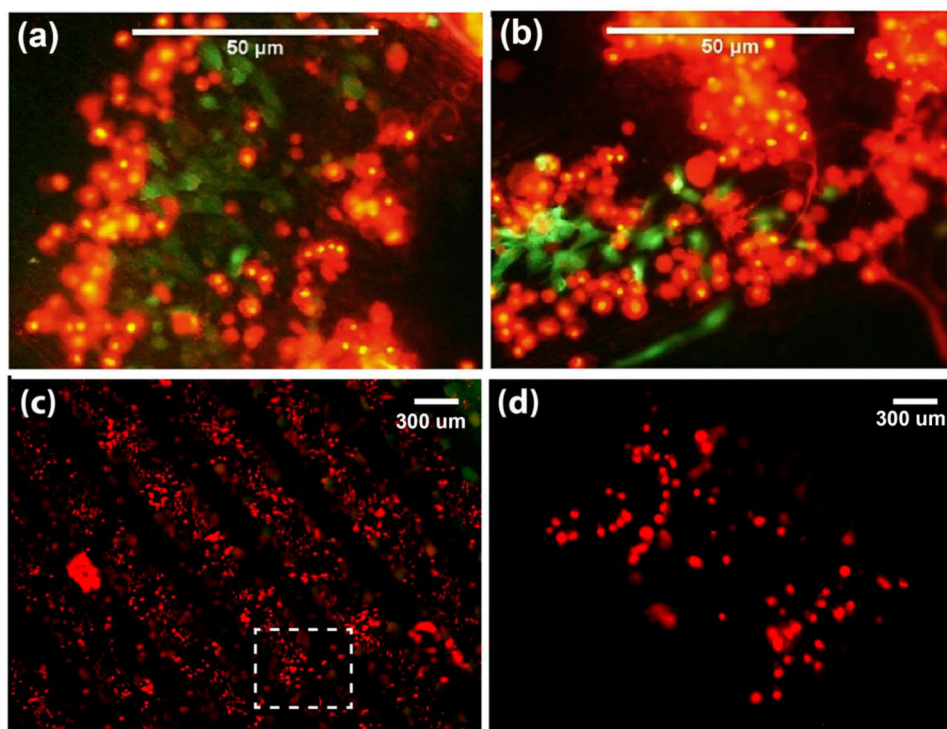


Figure 10. Optical fluorescent images for (a) AM Fe scaffolds made of truncated octahedron unit cell structure, (b) AM Fe scaffolds made of cubic shaped unit cell structure, (c) low-magnification fluorescent optical images of cells attached to AM Fe made of diamond unit cells and (d) higher magnification of the boxed area of the lattice structure in (c) [48,59].

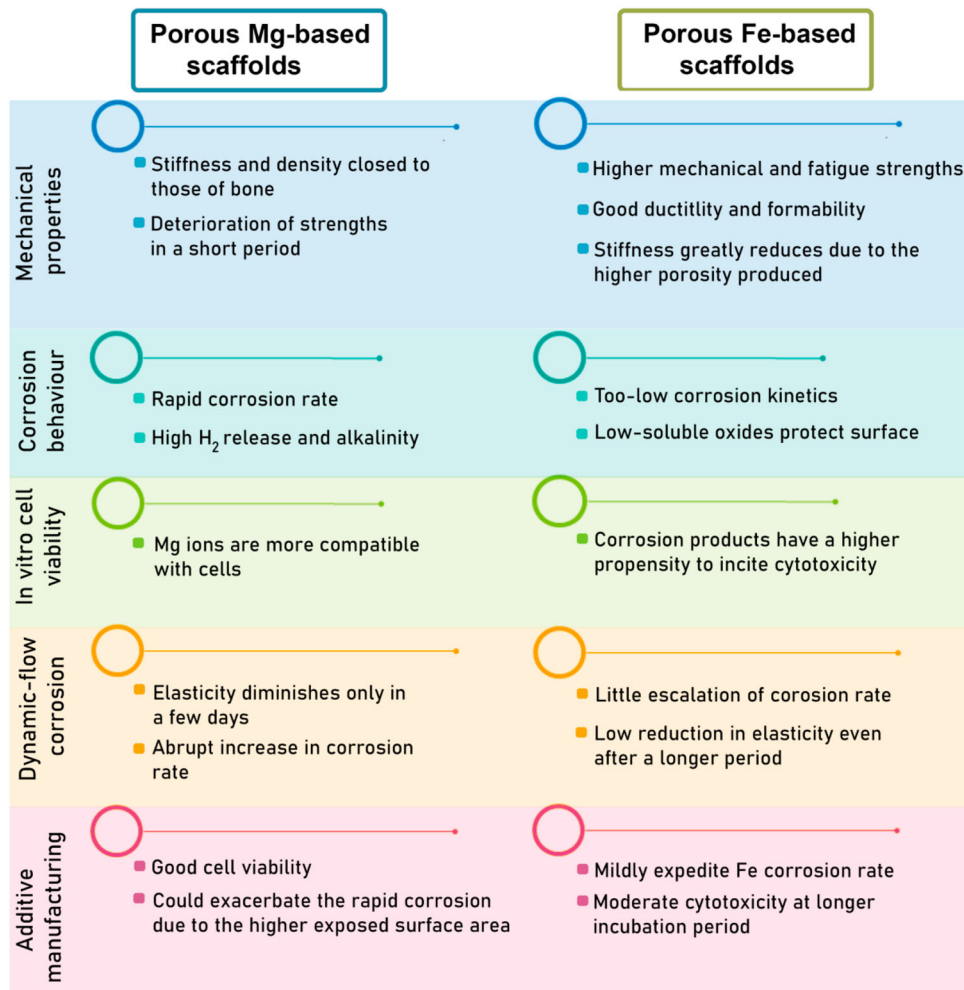


Figure 11. Current status of porous Mg-based and Fe-based scaffolds.

excessive Mg²⁺ concentration due to its rapid corrosion will pose detrimental effects on the cell growth and, therefore, they should be controlled accordingly. A great deal of study is always essential to fully evaluate its long-term corrosion–biocompatibility interactions *in vivo*. Based on the reviewed findings and the data in Table 4, it is clear that the porous Mg-based scaffold is highly depending on surface modifications or coating as evidenced by the corrosion resistance, biocompatibility and mechanical strengths. Thus, to overcome these issues, we suggest surface treatment of porous Mg scaffolds should be performed to control its excessive corrosion.

Cytotoxicity of porous Fe

Bulk pure Fe is renowned for its higher compressive and tensile strengths as well as for its high fatigue strength, which is essential in absorbing the natural stresses and loads experienced by the skeletal system [50]. The high strength and low corrosion rate of Fe provide a higher degree of freedom to modulate its porous structure for tuning the corrosion rate and meeting the requirement of the different strength and flexibility for bone scaffolds. Thus, designing Fe-based porous structure form could be advantageous owing to an enhanced kinetics of corrosion in slow-moving environments such as hard tissues. The previous elasticity data indicate that the production of porous Fe in a higher porosity comes at the expense of losing as-fabricated elasticity.

Accordingly, an optimised porosity must be sought when designing and producing porous Fe to attain a balance between adequate elasticity and expedited corrosion kinetics. Other than that, the control of released Fe ion concentration and oxide corrosion products should be a primary direction for future studies as the issues of cytotoxicity of Fe-based oxide corrosion products have still persist in the Fe-based scaffolds. The *in vitro* cell viability data indicate that the sign of cytotoxicity of porous Fe-based scaffolds could commence just after 24 h incubation and it could be more susceptible as the incubation period is prolonged. In this respect, it is worthwhile to consider controlling and reducing the high accumulation of the oxide and Fe ions in future *in vitro* and *in vivo* studies. Besides common surface modifications, the use of chelation chemistry to engage with the Fe ions in order to modulate the formation of oxide corrosion products are worth to be explored.

Uniform corrosion

Another big challenge in the corrosion aspect is to obtain uniform corrosion over the entire porous structure. The uniform corrosion is vital to ensure a concurrent gradual scaffold corrosion and an efficient new bone accommodation while preventing stress concentration and an implant failure. As per our review, studies focusing on the corrosion uniformity of Mg or Fe-based implants are limited [81,104] and none of them are in porous structure.

Uniform corrosion involves the continuous shifting of anode and cathode regions and thus, the corrosion proceeds at the approximately the same rate over the exposed surface. From our standpoint, it is hard for the metallic porous structure to exhibit the uniform corrosion even though Mg has a more propensity to undergo a more homogenous corrosion than Fe which is often associated with pitting corrosion [69,78]. The strut structure with curvy design in random open-pore porous scaffolds as well as the joints between the struts for topologically ordered scaffolds tend to be the crack initiation sources which greatly favour corrosion attack and thus, could lead to implant failure. In this respect, the corrosion uniformity should not be overlooked when designing the porous absorbable metals. Optimised architectural design parameters including the pore size, pore shape, porosity and curvature must be sought to avoid such premature scaffold failure. For porous Mg-based or Fe-based alloys, we suggest to develop single-phase alloys rather than multi-phase alloys to obtain a more uniform corrosion even though the former will show a higher corrosion resistance due to the declined galvanic corrosion.

Mechanical integrity concern

The elasticity data indicate that the elasticity of porous Mg-based and Fe-based scaffolds is highly on the porosity. Even though only elastic modulus data are present in this review which might not fully reflect the real mechanical performance of the scaffolds, it could raise a concern regarding scaffolds' mechanical integrity over corrosion period. As the elasticity could deteriorate to 1 GPa when the porosity approaches 70%, we expect that it is hard to achieve a sufficient mechanical retention over 12–24 weeks corrosion period since a higher porosity (>80) is always desired to enhance bone ingrowth and osseointegration of the implant after surgery. Based on the data, almost all of porous Mg-based and Fe-based scaffolds including the AM scaffolds exhibit lower stiffness than that of human cortical bone (7–27 GPa) [105]. In regard to this matter, we envisage that it is sensible to develop them for cancellous bone substitution rather than for cortical bone which necessitates higher mechanical strengths. Nevertheless, mechanical strengths of the porous metals can be escalated via several approaches. Before porous structure fabrication, the bulk metal could undergo strengthening techniques such as work hardening, age hardening and solid solution strengthening [105]. For AM scaffolds, optimum pore shape, porosity, geometry and unit cells used should be sought besides improving the AM processing parameters. If the high porosity is to be slightly compromised to retain an adequate strength over corrosion period, we suggest to perform modification on the metal surface via the surface functionalisation to counteract the biocompatibility loss.

Surface functionalisation

In order to augment the biocompatibility of porous absorbable metals, biochemical surface functionalisation could be applied on their surface. This involves the immobilisation of biomolecules that related in bone development and fracture healing such as proteins, peptides or enzymes onto metallic surfaces to induce and directly control bone tissue responses at the scaffold–tissue interface. For a better

functionalisation, covalent bonding can be developed between the biomolecules and the metallic surface to obtain a much stronger bonding and a long retention. In real environment, the linked biomolecules need to interact with the surrounding host tissue for a certain period of time, and thus a sustained retention promotes a fully activation of cellular responses. As per our review, there has been no surface biochemical functionalisation via covalent bonding performed on porous absorbable metallic scaffolds for bone scaffolds applications thus far, making it an interesting approach to be further explored. Besides the biochemicals, bioactive elements also could be loaded or incorporated into the pores to further enhance the biocompatibility.

Additive manufacturing

Mg-based powders have two main challenges in AM which are severe evaporation and high chemical reactivity in comparison to Fe-based powders. Besides, we are concern regarding its post-AM mechanical strengths as the elasticity substantially decreased to only 0.8 GPa. Even though it is still in the ranges of cancellous bone's elasticity (0.01–2 GPa), the AM porous Mg-based scaffolds (porous WE43 alloys) could suffer from a mechanical failure in a short period due to its own rapid corrosion attack. This mechanical failure could be worsened by the high exposed surface area and porosity provided by the topological design. Based on the reviewed data, the AM porous Mg alloys had a 20% volume loss after 4 weeks of corrosion period. It is improbable that the porous Mg alloys could retain the strengths for the required 12–24 weeks. This substantial strength loss coupled with the high exposed surface area could be the plausible contributing factors for the lack of AM studies on porous Mg-based scaffolds thus far, when compared with AM porous Fe-based scaffolds. The AM processing mildly enhanced the elasticity (0.5–2 GPa) and slightly escalated the corrosion rate of porous Fe. The mechanical strengths of the developed porous Fe and Mg could be further strengthened by several ways. Besides alloying and surface coating, optimisation of AM processing parameters and post-AM heat treatment could be performed to minimise the internal and defects such as thermal stresses and microstructural defects [105,106].

Further, the optimised architectural design including the unit cell, porosity, pore size, strut thickness, surface pattern, curvature and permeability [107,108] must be sought to produce a stable mechanical integrity with a balanced corrosion pace. Biocompatibility wise, the topological structure of the AM scaffolds has not directly facilitated the cell viability of both types of porous absorbable metals as no reports directly attributed the good cell viability, particularly for porous Mg-based scaffolds, to the architectural design and high pore interconnectivity of the AM scaffolds. For AM porous Fe, despite its slightly escalated corrosion rate, its moderate toxicity at longer incubation period as depicted in [Figure 10](#) suggests that the severity of the released corrosion products particularly excessive Fe^{2+} accumulation seems to surpass the favourable effect of high pore interconnectivity and uniform porosity provided by the AM Fe scaffolds. Thus, the factor of topological design on the enhancement of cell viability is still vague.

Dynamic vs. static immersion

The recent advent of dynamic immersion to characterise and analyse the corrosion behaviour is a highly beneficial development as it could mimic the real physiological environment in the human body, which involves the mass transfer across the scaffolds. From the data presented in this review, it can be seen that the corrosion rate of porous Mg-based scaffolds is very dependent on the type of experiment, dynamic or static immersion whereby the corrosion rate of porous Mg is sensitive to dynamic immersion; in other words, corrosion will be significantly accelerated if carried out under dynamic conditions. Such effect has not been prominently seen for Fe-based scaffolds due to its much slower anodic dissolution.

The use of common static immersion in corrosion evaluation tends to overestimate the corrosion rate and behaviour as well as the cytotoxicity effect of the porous scaffolds. The dynamic immersion could be a pre-requisite assessment to evaluate the corrosion as it yields a different corrosion response in comparison to the typical static immersion, as shown and discussed earlier. The corrosion rate especially for porous Mg and corrosion mechanism were shown to be differed between the static and dynamic immersion. The high sensitivity of porous Mg scaffolds towards the dynamic immersion could be a big problem since elevated porosity is often required and, on this account, porosity optimisation coupled with surface and microstructure alterations are worth to be considered to avoid scaffold failure both in mechanical integrity and biocompatibility aspects. For porous Fe, based on the satisfactory corrosion rate achieved in the short-term dynamic immersion, we suggest that material modification such as microstructural alteration via alloying is performed on the scaffold to maintain an adequate corrosion kinetics as the dense oxide corrosion products could often impede the corrosion progress.

Bioabsorption and biodistribution of the oxide products

In order to fully utilise the porous absorbable metals in clinical applications, the cellular biodegradation, bioabsorption and biodistribution of their oxide corrosion products released in the vicinity of the scaffolding area should be understood in-depth and clearly described first. Different Mg-based and Fe-based oxide species and oxide particle size have different surface potential and surface reactivity. In this regard, we can anticipate that the bioabsorption, biodistribution and clearance of the corrosion products species could be different. In addition, the size of oxide products could range from pico to macroscales. We believe that the oxide products of Mg-based and Fe-based scaffolds with micro and macro in sizes could be released, given that the porous structure is made of struts with high pore interconnectivity which are more susceptible to fracture. Bearing in mind that the surface reactivity of an oxide particle in its nano-size range differs from its microscale range with respect to the state of agglomeration, radical formation potential and cellular toxicity [109]. The smaller the oxide corrosion particles, the farther the distribution in the tissue will be [110]. On that account, the reliability and safety of the absorbable metals in the body considerably rely on the efficient bioabsorption and biodistribution of their corrosion products. The bioabsorption and biodistribution of Fe and

Mg oxide particles as well as their respective ions are already well described [111–114]. Nevertheless, those of the corrosion products particles which compose of Fe-based or Mg-based alloys are still vague. We believe that it could be more complex due to the presence of other metallic elements in the particles. This abstruse issue could be a future research direction to unravel more explicitly the bioabsorption and clearance of these alloy particles and other alloying elements ions as well.

Chelation of ions

In our view, the chelation chemistry offers a potential solution to reduce the formation of insoluble oxide products, given that the oxides are originated from their corresponding ions. Taking Fe as the case considering its predominant effect of insoluble corrosion products when compared with Mg counterparts, suitable Fe chelator which should be biocompatible can be used to capture the Fe ions. We believe that an appropriate design of Fe ions chelation will assist in reducing the formation of dense oxide products since the Fe chelation could result in a more soluble complex and enhanced solubility [115]. In this regard, the formation of dense Fe-based oxide can be reduced and the precipitation of the formed complex on the Fe surface also can be minimised simultaneously. This will escalate the Fe corrosion further and prevent the partake of Fe in the Fenton reaction and thus, minimising the generation of free radicals. However, appropriate amount of the chelators is highly essential to obtain feasible chelation effects. We opine that the Fe chelation will be inefficient if inadequate chelators are used since one molecule of chelator could only bind a certain number of Fe ions while its excessive presence will block the ion's ability to catalyse redox reactions. This requires a careful study coupled with an in-depth knowledge of surface chemistry and chelation chemistry subjects (Figure 11).

All in all, this review summarised the recent research progress of porous Mg-based and Fe-based metals for bone scaffolds application. In short, despite its much higher tolerance to bone tissue, its rapid corrosion still persists in porous Mg-based scaffolds especially in dynamic immersion as the mechanical integrity could significantly diminish within few days of corrosion period. Porous Fe achieves a satisfactory corrosion rate via the topologically ordered design which mildly enhances its elasticity but do not assist in its biocompatibility at a longer corrosion period. Note that its corrosion products are still problematic for a better biocompatibility. With the present data, it is sensible to develop porous Mg-based and Fe-based scaffolds for cancellous bone substitution due to their low elasticity which is not adequate to support the cortical bone. This review provides an insight into the current status of corrosion of porous Mg-based and Fe-based scaffolds. Research gaps have been identified, and future directions have been suggested to address the remaining challenges for the betterment of porous absorbable metals to serve as a highly efficient bone scaffold.

Acknowledgements

The authors gratefully acknowledge the Malaysian Ministry of Education and Universiti Teknologi Malaysia under the Long-Term Research Grant Scheme (R.K130000.734004L825).

Disclosure statement

No potential conflict of interest was reported by the author(s).

Funding

This work was supported by Ministry of Higher Education, Malaysia: [Grant Number Long-Term Research Grant Scheme (R.K130000.734004L825)].

References

- [1] Gordeladze JO, Haugen HJ, Lyngstadaas SP, et al. Bone tissue engineering: state of the art, challenges, and prospects. In: A Hasan, editor. *Tissue engineering for artificial organs*. Weinheim, Germany : Wiley-VCH Verlag GmbH & Co. KGaA; 2017. p. 525–551.
- [2] Yusop AH, Bakir AA, Shaharom NA, et al. Porous biodegradable metals for hard tissue scaffolds: a review. *Int J Biomater*. 2012;2012:641430.
- [3] Gorejová R, Haverová L, Oriňáková R, et al. Recent advancements in Fe-based biodegradable materials for bone repair. *J Mater Sci*. 2019;54(3):1913–1947.
- [4] Hermawan H. Updates on the research and development of absorbable metals for biomedical applications. *Prog Biomater*. 2018;7:93–110.
- [5] Wang X, Xu S, Zhou S, et al. Topological design and additive manufacturing of porous metals for bone scaffolds and orthopaedic implants: a review. *Biomaterials*. 2016;83:127–141.
- [6] Zheng YF, Gu XN, Witte F. Biodegradable metals. *Mater Sci Eng R: Rep*. 2014;77:1–34.
- [7] Venezuela J, Dargusch MS. The influence of alloying and fabrication techniques on the mechanical properties, biodegradability and biocompatibility of zinc: a comprehensive review. *Acta Biomater*. 2019;87:1–40.
- [8] Staiger MP, Pietak AM, Huadmai J, et al. Magnesium and its alloys as orthopedic biomaterials: a review. *Biomaterials*. 2006;27(9):1728–1734.
- [9] Yazdimamaghani M, Razavi M, Vashae D, et al. Porous magnesium-based scaffolds for tissue engineering. *Mater Sci Eng C*. 2017;71:1253–1266.
- [10] Yu W, Zhao H, Ding Z, et al. In vitro and in vivo evaluation of MgF2 coated AZ31 magnesium alloy porous scaffolds for bone regeneration. *Colloids Surf B*. 2017;149:330–340.
- [11] Mutlu I. Production and characterization of highly porous biodegradable Mg alloy scaffolds containing Ca, Zn and Co. *Biomed Mater Eng*. 2017;29(1):119–135.
- [12] Liu W, Wang J, Jiang G, et al. The improvement of corrosion resistance, biocompatibility and osteogenesis of the novel porous Mg-Nd-Zn alloy. *J Mater Chem B*. 2017;5(36):7661–7674.
- [13] Hong K, Park H, Kim Y, et al. Mechanical and biocorrosive properties of magnesium-aluminum alloy scaffold for biomedical applications. *J Mech Behav Biomed Mater*. 2019;98:213–224.
- [14] Dhyah A, Aprilia E, Franciska PL, et al. Microstructure and corrosion study of porous Mg–Zn–Ca alloy in simulated body fluid. *Mater Res Express*. 2017;4(3):034006.
- [15] Jia G, Chen C, Zhang J, et al. In vitro degradation behavior of Mg scaffolds with three-dimensional interconnected porous structures for bone tissue engineering. *Corros Sci*. 2018;144:301–312.
- [16] Md Saad AP, Syahrom A. Study of dynamic degradation behaviour of porous magnesium under physiological environment of human cancellous bone. *Corros Sci*. 2018;131:45–56.
- [17] Seyedraoufi ZS, Mirdamadi S. Microstructure, in vitro corrosion and mechanical properties of porous magnesium-zinc nanocomposite scaffolds. *Int J Res Mater Sci*. 2015;1(1):49–58.
- [18] Yazdimamaghani M, Razavi M, Vashae D, et al. In vitro analysis of Mg scaffolds coated with polymer/hydrogel/ceramic composite layers. *Surf Coat Technol*. 2016;301:126–132.
- [19] Kang M-H, Lee H, Jang T-S, et al. Biomimetic porous Mg with tunable mechanical properties and biodegradation rates for bone regeneration. *Acta Biomater*. 2019;84:453–467.
- [20] Katarivas Levy G, Ventura Y, Goldman J, et al. Cytotoxic characteristics of biodegradable EW10X04 Mg alloy after Nd coating and subsequent heat treatment. *Mater Sci Eng: C*. 2016;62:752–761.
- [21] Song G. Control of biodegradation of biocompatible magnesium alloys. *Corros Sci*. 2007;49(4):1696–1701.
- [22] Seitz J-M, Eifler R, Bach F-W, et al. Magnesium degradation products: effects on tissue and human metabolism. *J Biomed Mater Res A*. 2014;102(10):3744–3753.
- [23] Noviana D, Paramitha D, Ulum MF, et al. The effect of hydrogen gas evolution of magnesium implant on the postimplantation mortality of rats. *J Orthop Translat*. 2016;5:9–15.
- [24] Biezma MV. The role of hydrogen in microbiologically influenced corrosion and stress corrosion cracking. *Int J Hydrogen Energy*. 2001;26(5):515–520.
- [25] Mai ED, Liu H. Investigation on magnesium degradation under flow versus static conditions using a novel impedance-driven flow apparatus. *Prog Nat Sci Mater Int*. 2014;24(5):554–560.
- [26] Yazdimamaghani M, Razavi M, Vashae D, et al. Development and degradation behavior of magnesium scaffolds coated with polycaprolactone for bone tissue engineering. *Mater Lett*. 2014;132(Supplement C):106–110.
- [27] Li Y, Jahr H, Zhang XY, et al. Biodegradation-affected fatigue behavior of additively manufactured porous magnesium. *Addit Manuf*. 2019;28:299–311.
- [28] Li Y, Zhou J, Pavanram P, et al. Additively manufactured biodegradable porous magnesium. *Acta Biomater*. 2018;67:378–392.
- [29] Kopp A, Derra T, Mütter M, et al. Influence of design and post-processing parameters on the degradation behavior and mechanical properties of additively manufactured magnesium scaffolds. *Acta Biomater*. 2019;98:23–35.
- [30] Witte F, Jauer L, Meiners W, et al. Open-porous biodegradable magnesium scaffolds produced by selective laser melting for individualized bone replacement. *Front Bioeng Biotechnol*. 2016; *Biotechnol. Conference Abstract: 10th World Biomaterials Congress*.
- [31] Aghion E, Perez Y. Effects of porosity on corrosion resistance of Mg alloy foam produced by powder metallurgy technology. *Mater Charact*. 2014;96:78–83.
- [32] Md. Saad AP, Jasmawati N, Harun MN, et al. Dynamic degradation of porous magnesium under a simulated environment of human cancellous bone. *Corros Sci*. 2016;112:495–506.
- [33] Cheng M-Q, Wahafu T, Jiang G-F, et al. A novel open-porous magnesium scaffold with controllable microstructures and properties for bone regeneration. *Sci Rep*. 2016;6:24134.
- [34] Md Saad AP, Abdul Rahim RA, Harun MN, et al. The influence of flow rates on the dynamic degradation behaviour of porous magnesium under a simulated environment of human cancellous bone. *Mater Des*. 2017;122:268–279.
- [35] Seyedraoufi ZS, Mirdamadi S. Produce of biodegradable porous Mg-Zn scaffold via powder metallurgy and coated with nano HAP synthesized by electrodeposition process. *J Environ Friendly Mater*. 2017;1(1):40–45.
- [36] Mutlu I. Production and fluoride treatment of Mg-Ca-Zn-Co alloy foam for tissue engineering applications. *Trans Nonferrous Met Soc China*. 2018;28(1):114–124.
- [37] Bakhsheshi-Rad HR, Hamzah E, Staiger MP, et al. Drug release, cytocompatibility, bioactivity, and antibacterial activity of doxycycline loaded Mg-Ca-TiO₂ composite scaffold. *Mater Des*. 2018;139:212–221.
- [38] Md Saad AP, Prakoso AT, Sulong MA, et al. Impacts of dynamic degradation on the morphological and mechanical characterisation of porous magnesium scaffold. *Biomech Model Mechanobiol*. 2019;18(3):797–811.
- [39] Ghasali E, Bordbar-Khiabani A, Alizadeh M, et al. Corrosion behavior and in-vitro bioactivity of porous Mg/Al₂O₃ and Mg/Si₃N₄ metal matrix composites fabricated using microwave sintering process. *Mater Chem Phys*. 2019;225:331–339.
- [40] Singh S, Vashisth P, Shrivastav A, et al. Synthesis and characterization of a novel open cellular Mg-based scaffold for tissue engineering application. *J Mech Behav Biomed Mater*. 2019;94:54–62.
- [41] Toghiani S, Khodaei M, Razavi M. Magnesium scaffolds with two novel biomimetic designs and MgF₂ coating for bone tissue engineering. *Surf Coat Technol*. 2020;395:125929.
- [42] Yan Y, Kang Y, Li D, et al. Microstructure, mechanical properties and corrosion behavior of porous Mg-6 wt.% Zn scaffolds

- for bone tissue engineering. *J Mater Eng Perform.* **2018**;27(3):970–984.
- [43] Papanikolaou G, Pantopoulos K. Iron metabolism and toxicity. *Toxicol Appl Pharmacol.* **2005**;202(2):199–211.
- [44] Peuster M, Wohlsein P, Brüggemann M, et al. A novel approach to temporary stenting: degradable cardiovascular stents produced from corrodible metal—results 6–18 months after implantation into New Zealand white rabbits. *Heart.* **2001**;86(5):563–569.
- [45] Trumbo P, Schlicker S, Yates AA, et al. Dietary reference intakes for energy, carbohydrate, fiber, fat, fatty acids, cholesterol, protein and amino acids. *J Am Diet Assoc.* **2002**;102(11):1621–1630.
- [46] Schinhammer M, Gerber I, Hännzi AC, et al. On the cytocompatibility of biodegradable Fe-based alloys. *Mater Sci Eng C.* **2013**;33(2):782–789.
- [47] Yusop AH, Sarian MN, Januddi FS, et al. Structure, degradation, drug release and mechanical properties relationships of iron-based drug eluting scaffolds: the effects of PLGA. *Mater Des.* **2018**;160:203–217.
- [48] Sharma P, Jain KG, Pandey PM, et al. In vitro degradation behaviour, cytocompatibility and hemocompatibility of topologically ordered porous iron scaffold prepared using 3D printing and pressureless microwave sintering. *Mater Sci Eng C.* **2020**;106:110247.
- [49] Kraus T, Moszner F, Fischerauer S, et al. Biodegradable Fe-based alloys for use in osteosynthesis: outcome of an in vivo study after 52 weeks. *Acta Biomater.* **2014**;10(7):3346–3353.
- [50] Heiden M, Walker E, Stanciu L. Magnesium, iron and zinc alloys, the trifecta of bioresorbable orthopaedic and vascular implantation—a review. *J Biotechnol Biomater.* **2015**;5:2–9.
- [51] Hrubovčáková M, Kupková M, Džupon M. Fe and Fe-P foam for biodegradable bone replacement material: morphology, corrosion behaviour, and mechanical properties. *Adv Mater Sci Eng.* **2016**: Article ID 6257368.
- [52] Feng YP, Gaztelumendi N, Fornell J, et al. Mechanical properties, corrosion performance and cell viability studies on newly developed porous Fe-Mn-Si-Pd alloys. *J Alloys Compd.* **2017**;724:1046–1056.
- [53] Hong D, Chou D-T, Velikokhatnyi OI, et al. Binder-jetting 3D printing and alloy development of new biodegradable Fe-Mn-Ca/Mg alloys. *Acta Biomater.* **2016**;45:375–386.
- [54] Hrubovčáková M, Kupková M, Džupon M, et al. Biodegradable polylactic acid and poly(lactic acid/hydroxyapatite) coated iron foams for bone replacement materials. *Int J Electrochem Sci.* **2017**;12:11122–11136.
- [55] Oriňáková R, Gorejová R, Macko J, et al. Evaluation of in vitro biocompatibility of open cell iron structures with PEG coating. *Appl Surf Sci.* **2019**;475:515–518.
- [56] Yusop A, Daud N, Hermawan H. Development of PLGA-infiltrated porous iron for temporary medical implants. *Eur Cells Mater.* **2013**;26:9.
- [57] Yusop AH, Hermawan H. Synthesis and development of polymers-infiltrated porous iron for temporary medical implants: a preliminary result. *Adv Mat Res.* **2013**;686:331–335.
- [58] Huang SM, Nauman EA, Stanciu LA. Investigation of porosity on mechanical properties, degradation and in-vitro cytotoxicity limit of Fe₃₀Mn using space holder technique. *Mater Sci Eng: C.* **2019**;99:1048–1057.
- [59] Li Y, Jahr H, Lietaert K, et al. Additively manufactured biodegradable porous iron. *Acta Biomater.* **2018**;77:380–393.
- [60] Sharma P, Pandey PM. Morphological and mechanical characterization of topologically ordered open cell porous iron foam fabricated using 3D printing and pressureless microwave sintering. *Mater Des.* **2018**;160:442–454.
- [61] Sharma P, Pandey PM. A novel manufacturing route for the fabrication of topologically-ordered open-cell porous iron scaffold. *Mater Lett.* **2018**;222:160–163.
- [62] Li Y, Lietaert K, Li W, et al. Corrosion fatigue behavior of additively manufactured biodegradable porous iron. *Corros Sci.* **2019**;156:106–116.
- [63] Chou D-T, Wells D, Hong D, et al. Novel processing of iron-manganese alloy-based biomaterials by inkjet 3-D printing. *Acta Biomater.* **2013**;9(10):8593–8603.
- [64] Li Y, Jahr H, Pavanram P, et al. Additively manufactured functionally graded biodegradable porous iron. *Acta Biomater.* **2019**;96:646–661.
- [65] Obayi CS, Tolouei R, Mostavan A, et al. Effect of grain sizes on mechanical properties and biodegradation behavior of pure iron for cardiovascular stent application. *Biomater.* **2016**;6(1):e959874.
- [66] Shuai C, Yang W, Yang Y, et al. Selective laser melted Fe-Mn bone scaffold: microstructure, corrosion behavior and cell response. *Mater Res Express.* **2020**;7(1):015404.
- [67] Yang C, Huan Z, Wang X, et al. 3D printed Fe scaffolds with HA nanocoating for bone regeneration. *ACS Biomater Sci Eng.* **2018**;4(2):608–616.
- [68] Mohd Daud N, Sing NB, Yusop AH, et al. Degradation and in vitro cell-material interaction studies on hydroxyapatite-coated biodegradable porous iron for hard tissue scaffolds. *J Orthop Translat.* **2014**;2(4):177–184.
- [69] Yusop AHM, Daud NM, Nur H, et al. Controlling the degradation kinetics of porous iron by poly(lactic-co-glycolic acid) infiltration for use as temporary medical implants. *Sci Rep.* **2015**;5:11194.
- [70] He J, He F-L, Li D-W, et al. A novel porous Fe/Fe-W alloy scaffold with a double-layer structured skeleton: preparation, in vitro degradability and biocompatibility. *Colloids Surf B.* **2016**;142:325–333.
- [71] Orinakova R, Orinak A, Buckova LM, et al. Iron based degradable foam structures for potential orthopedic applications. *Int J Electrochem Sci.* **2013**;8(12):12451–12465.
- [72] Feng YP, Blanquer A, Fornell J, et al. Novel Fe–Mn–Si–Pd alloys: insights into mechanical, magnetic, corrosion resistance and biocompatibility performances. *J Mater Chem B.* **2016**;4(39):6402–6412.
- [73] Su Y, Champagne S, Trenggono A, et al. Development and characterization of silver containing calcium phosphate coatings on pure iron foam intended for bone scaffold applications. *Mater Des.* **2018**;148:124–134.
- [74] Sharma P, Pandey PM. Corrosion behaviour of the porous iron scaffold in simulated body fluid for biodegradable implant application. *Mater Sci Eng C.* **2019**;99:838–852.
- [75] Sharma P, Pandey PM. Corrosion rate modelling of biodegradable porous iron scaffold considering the effect of porosity and pore morphology. *Mater Sci Eng: C.* **2019**;103:109776.
- [76] Carluccio D, Xu C, Venezuela J, et al. Additively manufactured iron-manganese for biodegradable porous load-bearing bone scaffold applications. *Acta Biomater.* **2020**;103:346–360.
- [77] Wang H, Zheng Y, Liu J, et al. In vitro corrosion properties and cytocompatibility of Fe-Ga alloys as potential biodegradable metallic materials. *Mater Sci Eng C.* **2017**;71:60–66.
- [78] Chen Y, Zhang W, Maitz MF, et al. Comparative corrosion behavior of Zn with Fe and Mg in the course of immersion degradation in phosphate buffered saline. *Corros Sci.* **2016**;111:541–555.
- [79] Huang T, Cheng J, Bian D, et al. Fe–Au and Fe–Ag composites as candidates for biodegradable stent materials. *J Biomed Mater Res Part B: Appl Biomater.* **2016**;104(2):225–240.
- [80] Moravej M, Prima F, Fiset M, et al. Electroformed iron as new biomaterial for degradable stents: development process and structure-properties relationship. *Acta Biomater.* **2010**;6(5):1726–1735.
- [81] Cheng J, Huang T, Zheng YF. Relatively uniform and accelerated degradation of pure iron coated with micro-patterned Au disc arrays. *Mater Sci Eng: C.* **2015**;48:679–687.
- [82] Huang T, Zheng Y. Uniform and accelerated degradation of pure iron patterned by Pt disc arrays. *Sci Rep.* **2016**;6:23627.
- [83] Obayi CS, Tolouei R, Paternoster C, et al. Influence of cross-rolling on the micro-texture and biodegradation of pure iron as biodegradable material for medical implants. *Acta Biomater.* **2015**;17:68–77.
- [84] Zadpoor AA. Mechanical performance of additively manufactured meta-biomaterials. *Acta Biomater.* **2019**;85:41–59.
- [85] Qin Y, Wen P, Guo H, et al. Additive manufacturing of biodegradable metals: current research status and future perspectives. *Acta Biomater.* **2019**;98:3–22.
- [86] Li Z-G, Zhang X-G, Huang P, et al. Preparation and properties of open-cell zinc foams as human bone substitute material. *China Foundry.* **2019**;16(6):414–422.
- [87] Yazdimaghani M, Razavi M, Vashae D, et al. Surface modification of biodegradable porous Mg bone scaffold using

- polycaprolactone/bioactive glass composite. *Mater Sci Eng C*. 2015;49:436–444.
- [88] Witte F, Kaese V, Haferkamp H, et al. In vivo corrosion of four magnesium alloys and the associated bone response. *Biomaterials*. 2005;26(17):3557–3563.
- [89] Li Y, Jahr H, Lietaert K, et al. Additively manufactured biodegradable porous iron. *Acta Biomater*. 2018;77:380–393.
- [90] Liu C, Wang J, Gao C, et al. Enhanced osteoinductivity and corrosion resistance of dopamine/gelatin/rhBMP-2-coated β -TCP/Mg-Zn orthopedic implants: an in vitro and in vivo study. *PLoS ONE*. 2020;15(1):e0228247.
- [91] Zhang Y-Q, Li Y, Liu H, et al. Mechanical and biological properties of a biodegradable Mg-Zn-Ca porous alloy. *Orthop Surg*. 2018;10(2):160–168.
- [92] Oriňák A, Oriňáková R, Králová ZO, et al. Sintered metallic foams for biodegradable bone replacement materials. *J Porous Mater*. 2014;21(2):131–140.
- [93] Scarcello E, Herpain A, Tomatis M, et al. Hydroxyl radicals and oxidative stress: the dark side of Fe corrosion. *Colloids Surf B*. 2019;110542.
- [94] He YF, Ma Y, Gao C, et al. Iron overload inhibits osteoblast biological activity through oxidative stress. *Biol Trace Elem Res*. 2013;152(2):292–296.
- [95] Fagali NS, Grillo CA, Puntarulo S, et al. Is there any difference in the biological impact of soluble and insoluble degradation products of iron-containing biomaterials? *Colloids Surf B*. 2017;160:238–246.
- [96] Zhu S, Huang N, Xu L, et al. Biocompatibility of pure iron: in vitro assessment of degradation kinetics and cytotoxicity on endothelial cells. *Mater Sci Eng: C*. 2009;29(5):1589–1592.
- [97] Zhang E, Chen H, Shen F. Biocorrosion properties and blood and cell compatibility of pure iron as a biodegradable biomaterial. *J Mater Sci: Mater Med*. 2010;21(7):2151–2163.
- [98] Li Y, Liu X, Tan L, et al. Enoxacin-loaded poly (lactic-co-glycolic acid) coating on porous magnesium scaffold as a drug delivery system: antibacterial properties and inhibition of osteoclastic bone resorption. *J Mater Sci Technol*. 2016;32(9):865–873.
- [99] Kang M-H, Jang T-S, Kim SW, et al. MgF₂-coated porous magnesium/alumina scaffolds with improved strength, corrosion resistance, and biological performance for biomedical applications. *Mater Sc Eng C*. 2016;62:634–642.
- [100] Hakimi O, Ventura Y, Goldman J, et al. Porous biodegradable EW62 medical implants resist tumor cell growth. *Mater Sci Eng C*. 2016;61:516–525.
- [101] Seyedraoufi ZS, Mirdamadi S. In vitro biodegradability and biocompatibility of porous Mg-Zn scaffolds coated with nano hydroxyapatite via pulse electrodeposition. *Trans Nonferrous Met Soc China*. 2015;25(12):4018–4027.
- [102] Kang M-H, Lee H, Jang T-S, et al. Biomimetic porous Mg with tunable mechanical properties and biodegradation rates for bone regeneration. *Acta Biomater*. 2019;84:453–467.
- [103] Yang Y, Zhou J, Detsch R, et al. Biodegradable nanostructures: degradation process and biocompatibility of iron oxide nanostructured arrays. *Mater Sci Eng C*. 2018;85:203–213.
- [104] Mao L, Yuan G, Wang S, et al. A novel biodegradable Mg–Nd–Zn–Zr alloy with uniform corrosion behavior in artificial plasma. *Mater Lett*. 2012;88:1–4.
- [105] Li Y, Jahr H, Zhou J, et al. Additively manufactured biodegradable porous metals. *Acta Biomater*. 2020;115:29–50.
- [106] Sezer N, Evis Z, Koç M. Additive manufacturing of biodegradable magnesium implants and scaffolds: review of the recent advances and research trends. *J Magnesium Alloys*. 2020; Advance online publication. doi:10.1016/j.jma.2020.09.014
- [107] Li Y, Roohani I, Li G, et al. Architectural design of 3D printed scaffolds controls the volume and functionality of newly formed bone. *Adv Healthc Mater*. 2019;8(1):1801353.
- [108] Callens SJP, Uyttendaele RJC, Fratila-Apachitei LE, et al. Substrate curvature as a cue to guide spatiotemporal cell and tissue organization. *Biomaterials*. 2020;232:119739.
- [109] Bhattacharya K, Hoffmann E, Schins RFP, et al. Comparison of micro- and nanoscale Fe+3-containing (hematite) particles for their toxicological properties in human lung cells in vitro. *Toxicol Sci*. 2012;126(1):173–182.
- [110] Paramitha D, Estuningsih S, Noviana D, et al. Distribution of Fe-based degradable materials in mice skeletal muscle. *European Cells Mater*. 2013;26:55.
- [111] Mangalampalli B, Dumala N, Perumalla Venkata R, et al. Genotoxicity, biochemical, and biodistribution studies of magnesium oxide nano and microparticles in albino wistar rats after 28-day repeated oral exposure. *Environ Toxicol*. 2018;33(4):396–410.
- [112] Feng Q, Liu Y, Huang J, et al. Uptake, distribution, clearance, and toxicity of iron oxide nanoparticles with different sizes and coatings. *Sci Rep*. 2018;8(1):2082.
- [113] Arami H, Khandhar A, Liggitt D, et al. In vivo delivery, pharmacokinetics, biodistribution and toxicity of iron oxide nanoparticles. *Chem Soc Rev*. 2015;44j(23):8576–8607.
- [114] Mittag A, Schneider T, Westermann M, et al. Toxicological assessment of magnesium oxide nanoparticles in HT29 intestinal cells. *Arch Toxicol*. 2019;93(6):1491–1500.
- [115] Norén K, Loring JS, Bargar JR, et al. Adsorption mechanisms of EDTA at the water–iron oxide interface: implications for dissolution. *J Phys Chem C*. 2009;113(18):7762–7771.